

1  
2  
3 **Probing the acid sites of zeolites with pyridine: quantitative AGIR**  
4 **measurements of the molar absorption coefficients**

5  
6 **Supplementary Information**  
7  
8

9 Vladimir Zholobenko <sup>a,b</sup> \*, Cátia Freitas <sup>b</sup>, Martin Jendrlin <sup>b</sup>, Philippe Bazin <sup>a</sup>, Arnaud Travert <sup>a</sup>,  
10 Frederic Thibault-Starzyk <sup>a</sup>

11  
12 <sup>a</sup> Normandie Univ, ENSICAEN, UNICAEN, CNRS, Laboratoire Catalyse et Spectrochimie, France

13 <sup>b</sup> School of Chemical and Physical Sciences, Keele University, United Kingdom

14  
15  
16  
17  
18 \* Corresponding author: v.l.zholobenko@keele.ac.uk

21           **Experimental**

22           List of Materials.

23           BEA-12 (Zeolyst CP814E, NH<sub>4</sub>-form, Si/Al=12.5)

24           BEA-19 (Zeolyst CP814C, NH<sub>4</sub>-form, Si/Al=19)

25           ZSM-5-40 (Zeolyst CBV8014, NH<sub>4</sub>-form, Si/Al=40)

26           ZSM-5-27 (NIST reference material RM8852, NH<sub>4</sub>-form, Si/Al=27)

27           MOR-7 (Crosfield, NH<sub>4</sub>-form, Si/Al=7.0)

28           MOR-10 (Zeolyst CBV21A, NH<sub>4</sub>-form, Si/Al=10)

29           FAU-C (Crosfield, NH<sub>4</sub>-form, Si/Al=2.6)

30           FAU-Z (Zeolyst CBV300, NH<sub>4</sub>-form, Si/Al=2.6)

31           γ-alumina (Puralox, Sasol)

32           fumed silica (Sigma-Aldrich, 99.8%)

33           US-Y zeolite (Crosfield, Si/Al=6)

34           The ex situ calcination temperature (if any) is indicated in the sample name. For instance,  
35           BEA-12-600°C refers to a CP814E zeolite calcined ex situ at 600°C prior to further analyses, the  
36           latter may have included an in situ activation at 450°C.

37           Details of the analytical procedures and instrumentation along with the characterisation data  
38           for the samples studied in this work, including XRD patterns, SEM images, NMR and FTIR  
39           spectroscopic data are presented below.

40           Powder X-ray diffraction (XRD) patterns were recorded on a Bruker D8 Advance  
41           diffractometer equipped with a LynxEye detector using Cu K $\alpha$  radiation at 40 kV and 40 mA at  
42           ambient temperature over the 2-θ angle range of 5-60° ( $\lambda_{K\alpha 1}=0.15406$  nm and  $\lambda_{K\alpha 2}=0.15444$  nm;  
43           Soller slit of 2.5°; step size of 0.02°; time per step of 2976 sec; no monochromator was used). The  
44           crystalline phases were matched by comparing the collected XRD patterns with those available in  
45           the literature.

46           TM3000 (Hitachi) scanning electron microscope (SEM) with energy dispersive X-ray analysis  
47           (EDX) was utilised to obtain the elemental composition of the catalysts.

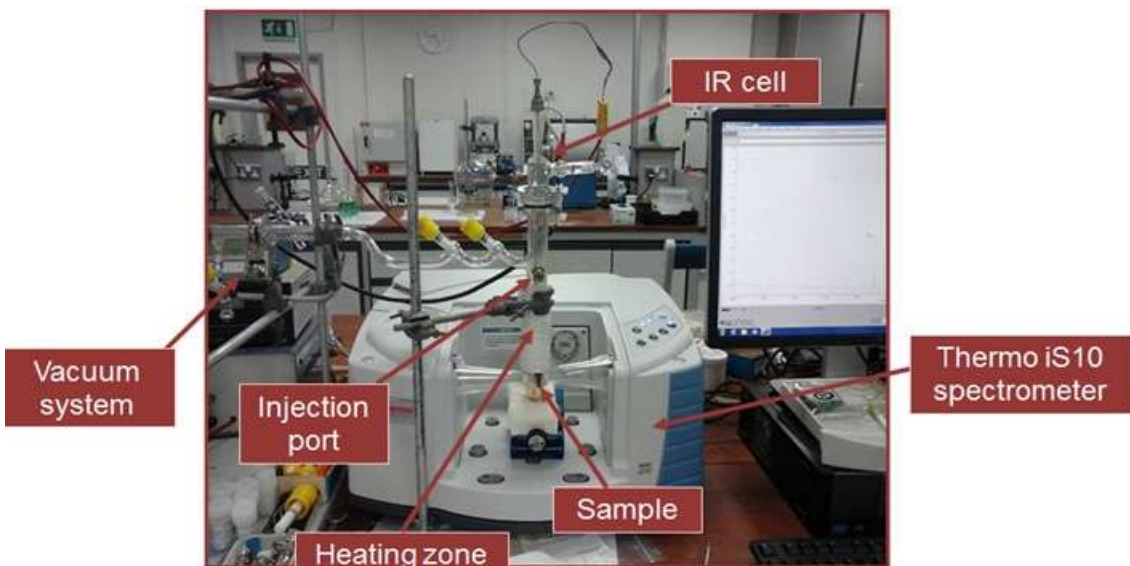
48           The apparent surface areas of the catalysts were measured using the BET model for the P/P<sub>0</sub>  
49           relative nitrogen pressure <0.04; their micropore volume and the pore size distribution were  
50           computed using the nonlinear density functional theory (NLDFT) model applied to the adsorption  
51           branch of the nitrogen adsorption isotherms, according to the recent IUPAC recommendations (M.  
52           Thommes, K. Kaneko, A.V. Neimark, J.P. Olivier, F. Rodriguez-Reinoso, J. Rouquerol and K.S.W.  
53           Sing, *Physisorption of gases, with special reference to the evaluation of surface area and pore size*  
54           *distribution (IUPAC Technical Report)*, Pure Appl. Chem., 2015, 87(9-10) 1051–1069). The

55 experiments were carried out on a Quantachrom Autosorb instrument. The values obtained were  
56 scaled to the mass of the activated samples.

57 The thermogravimetric analyses have been carried out using a Rheometric Scientific STA  
58 1500 instrument. The sample mass change and the heat flow were measured as a function of  
59 temperature (ramped from 20 to 800°C at 10°C/min).

60 Solid-state NMR experiments were performed using a 500 MHz Bruker Advance III  
61 spectrometer operating at a Larmor frequency of 130.3 MHz for  $^{27}\text{Al}$  and 99.3 MHz for  $^{29}\text{Si}$ .  
62 Hydrated powdered samples were packed into 4 mm rotors. For  $^{27}\text{Al}$  MAS NMR, spectra were  
63 acquired using a relatively short pulse length of 1  $\mu\text{s}$  (i.e., a selective pulse of 10°), a recycle delay  
64 of 1 s and a spinning rate of 14 kHz. For  $^{29}\text{Si}$  MAS NMR, spectra were acquired using a 30° pulse, a  
65 recycle delay of 20 s and a spinning rate of 12 kHz. Chemical shifts were referenced to 1 mol L<sup>-1</sup>  
66 Al(NO<sub>3</sub>)<sub>3</sub> solution for  $^{27}\text{Al}$  and to TMS for  $^{29}\text{Si}$ .

67



68  
69 **Figure S1.** *In situ* FTIR spectroscopy set-up at Keele University.

70



71

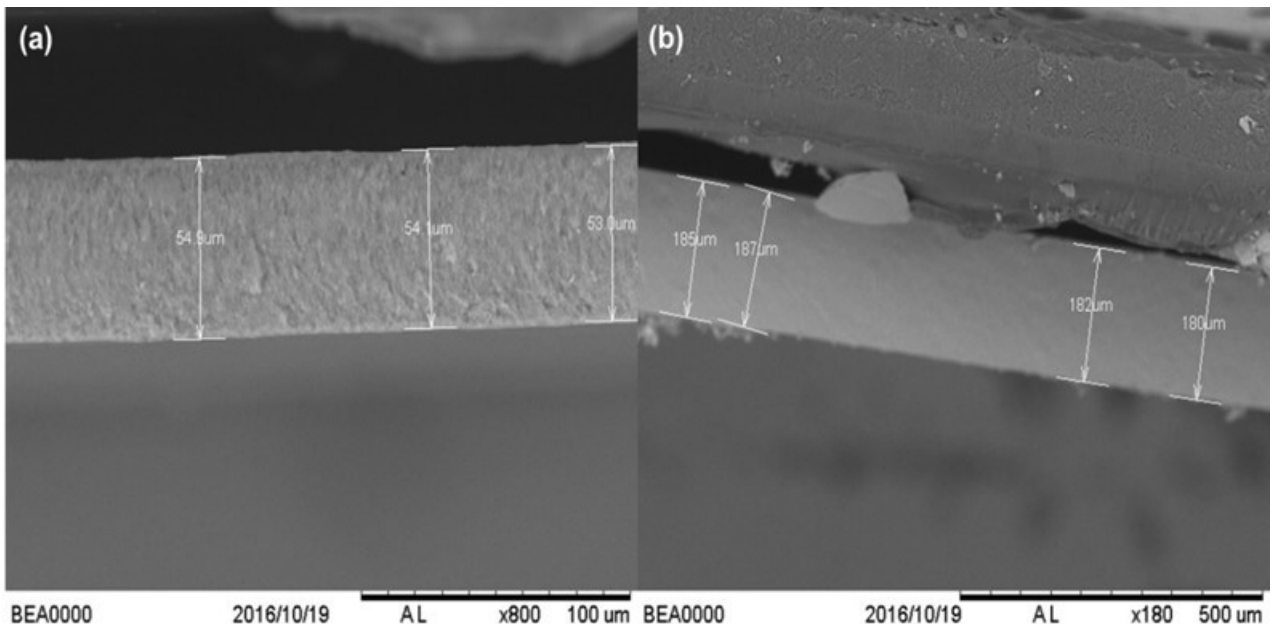
72 **Figure S2.** AGIR set-up at LCS, Caen.

73

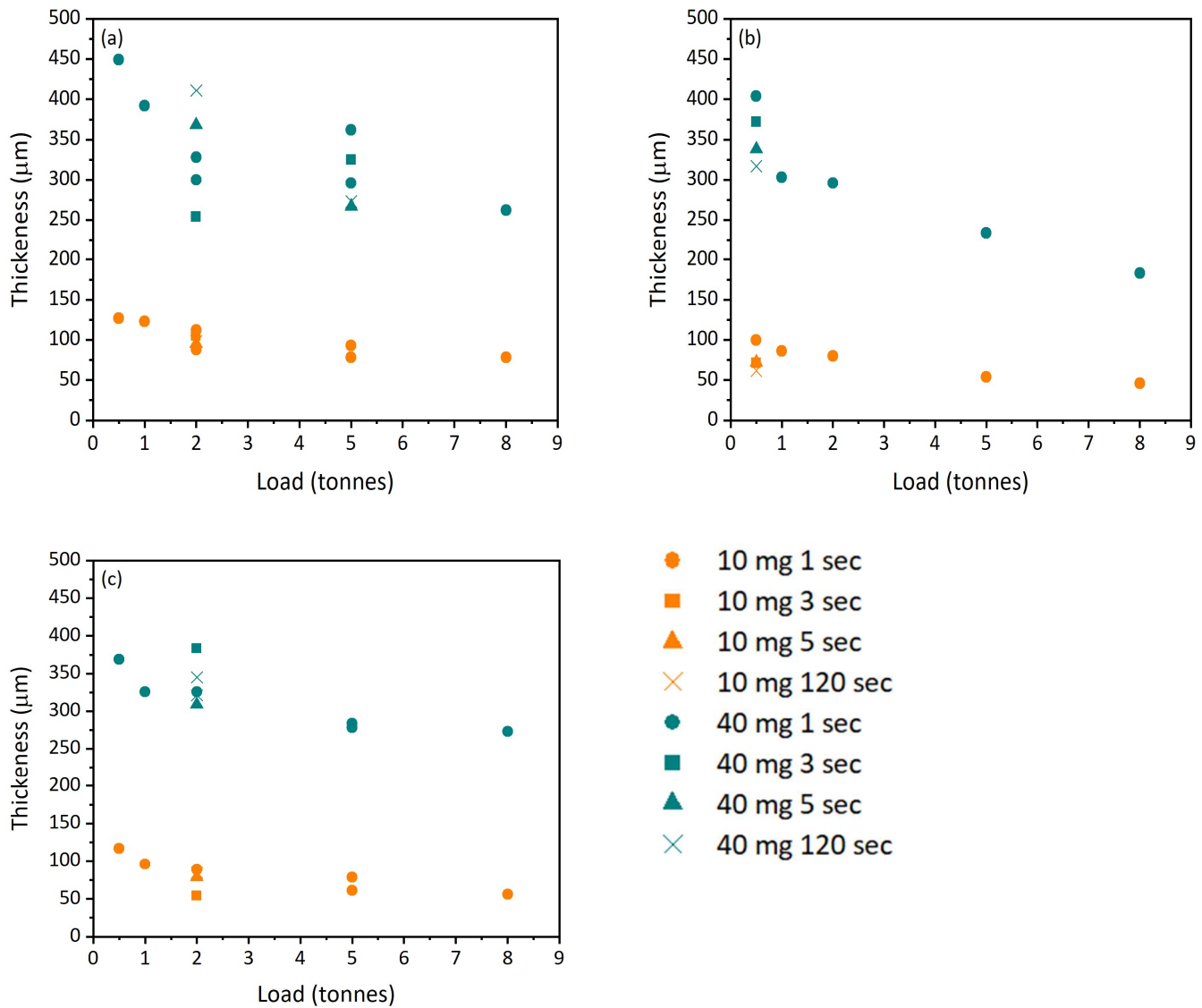
74           **Results and Discussion**

75           *Preparation of the self-supported discs for FTIR measurements*

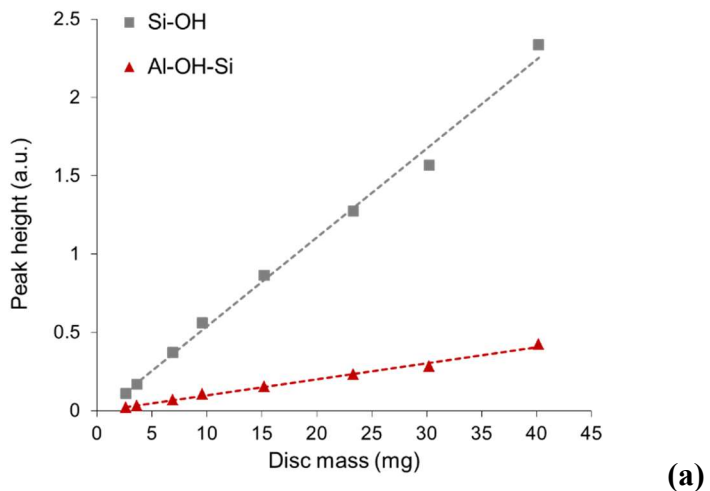
76           The selected materials (e.g., silica, BEA and ZSM-5-40 zeolites) were pressed into self-  
77 supporting discs with the cross-section of  $S=1.3\text{ cm}^2$ , using a hydraulic bench press. The discs were  
78 made using a different mass (~2-40 mg), load (0, 1, 2, 5 and 8 tonnes) and time under load (1, 3, 5  
79 and 120 sec). The SEM images were utilised to measure the thickness of the self-supporting discs.  
80 Figure S3 presents two SEM micrograph collected to obtain thickness data. Thickness of the disc  
81 decreases with increasing loads for all selected materials (fumed silica, BEA-12 and ZSM-5-40) and  
82 this effect is more noticeable for heavier discs (40 mg) (Figure S4). The changes are also observed  
83 when the discs are pressed at a different time under load, especially for the 40 mg discs. There are  
84 no significant changes in the thickness of the discs weighing ~10 mg after 5 seconds under pressure.  
85 These conclusions are similar for all materials selected for this study.



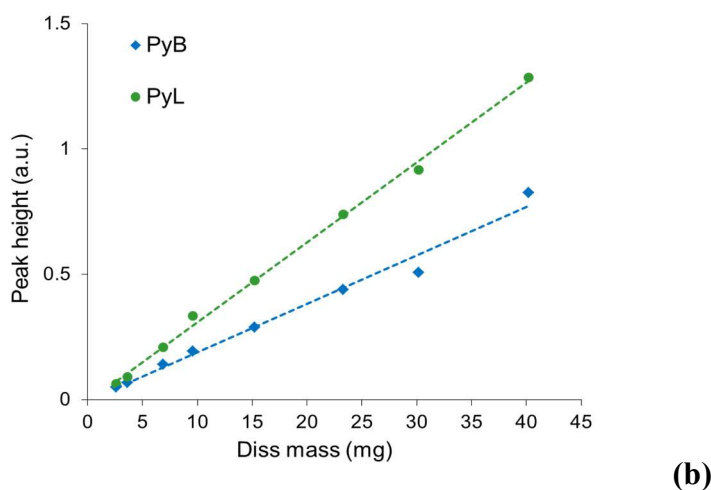
86           **Figure S3.** SEM micrograph of self-supported BEA-12 discs at different resolutions. (a) 10 mg  
87 BEA-12 sample prepared at an 8-tonne load for 1 sec and (b) 40 mg BEA-12 sample prepared at an  
88 8-tonne load for 1 sec.



95 **Figure S4.** Thickness of the self-supporting discs prepared at different mass, load and time under  
96 load. **(a)** fumed silica, **(b)** BEA-12, **(c)** ZSM-5-40 zeolites.



(a)



(b)

**Figure S5.** Linear relationship between the zeolite disc mass and the peak-height absorbance of the IR bands of (a) OH groups and (b) Py adsorbed on BAS and LAS in BEA-12 zeolite.

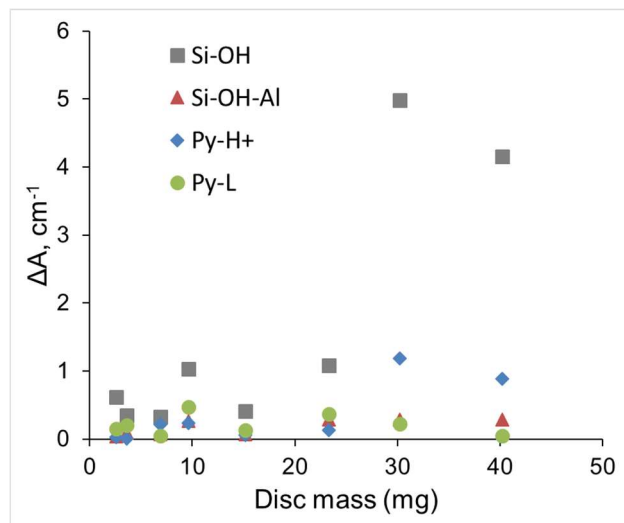
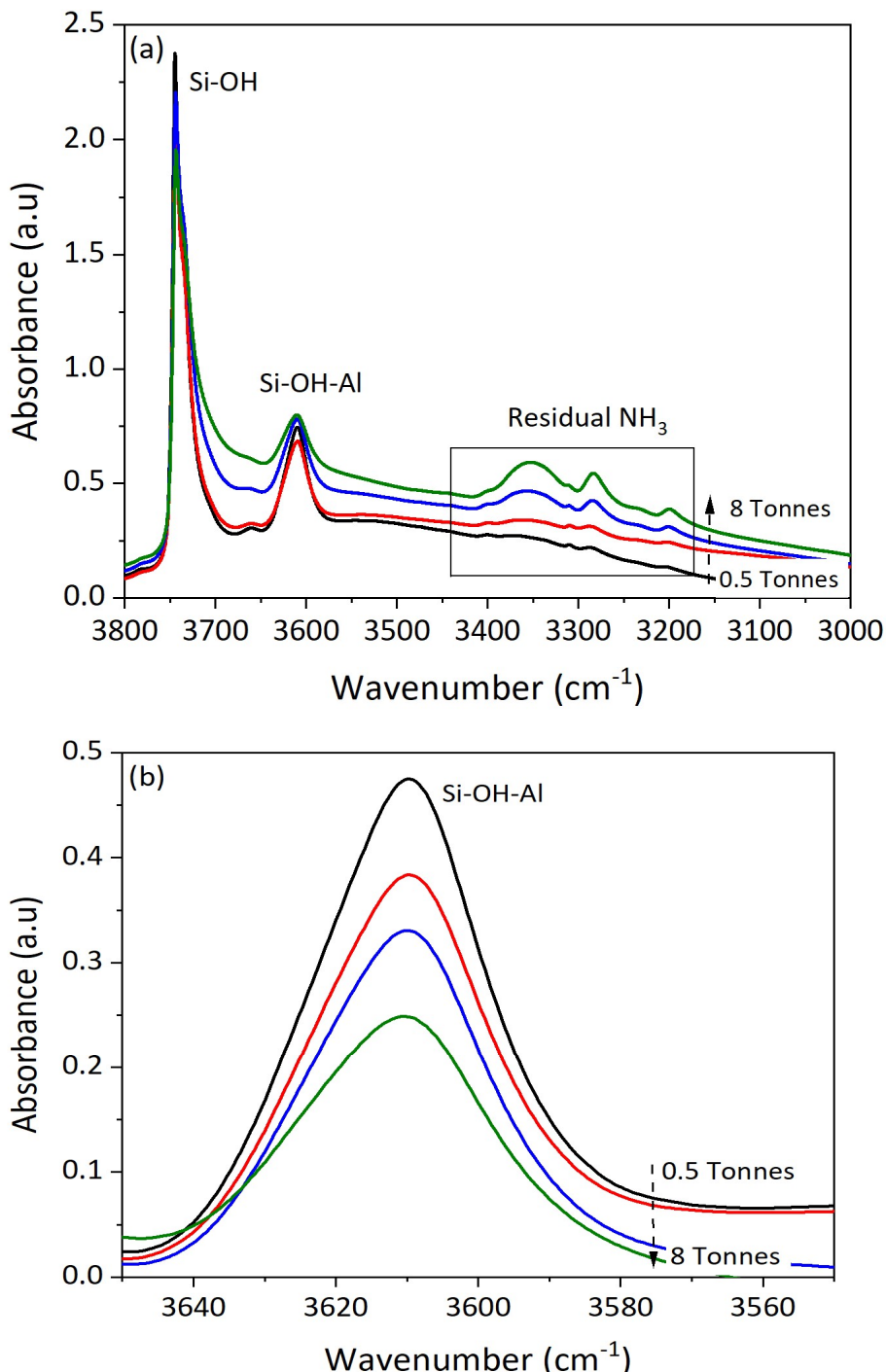


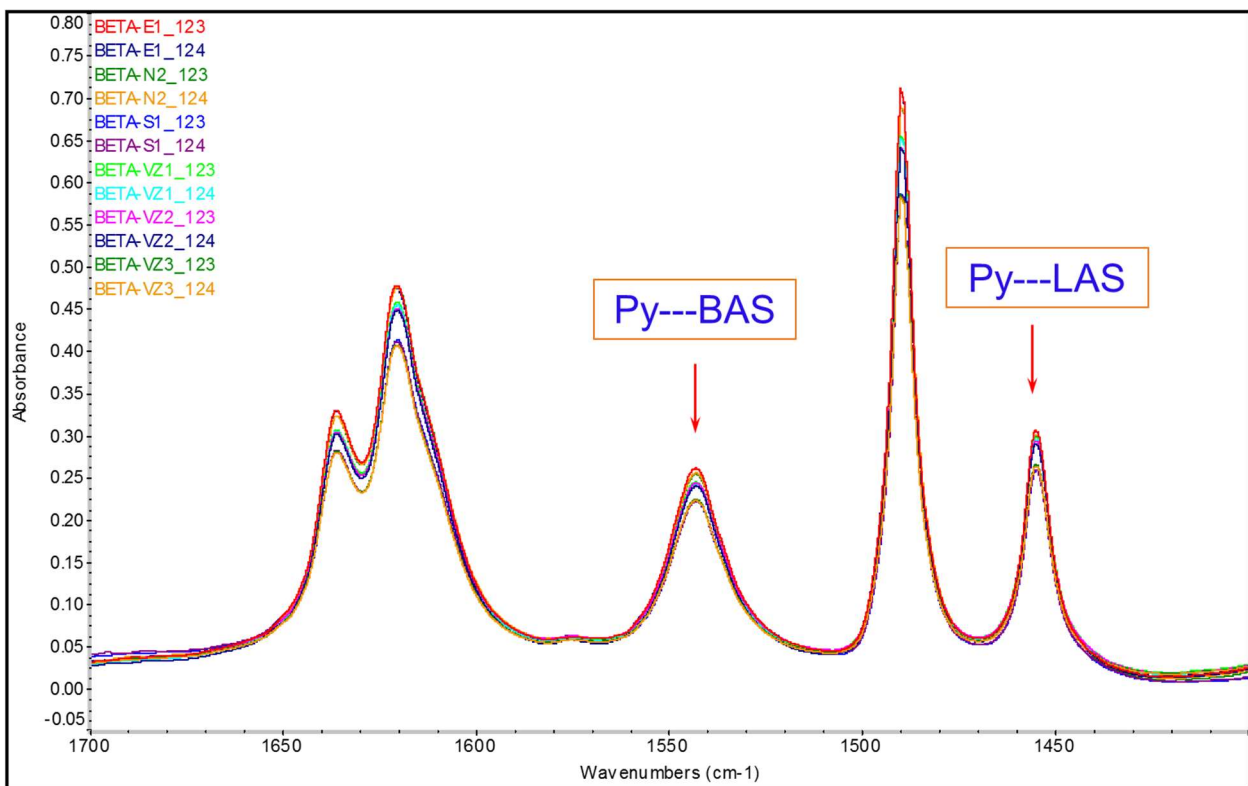
**Figure S6.** Deviation from the Beer-Lambert-Bouguer law for zeolite samples of different mass. (Based on the data presented in Figure 3;  $\Delta A$  refers to peak area as in Figure 3.

100        *Incomplete activation of the self-supporting sample discs prepared under the increasing load*  
 101        (0.5-8 tonnes) is evidenced by a decrease in the intensity of the Si-OH-Al peak at  $\sim 3610 \text{ cm}^{-1}$   
 102        (subsequent Py adsorption shows a reduction in the intensity of the of Py-B peak at  $\sim 1545 \text{ cm}^{-1}$ ).  
 103        This is due to the residual ammonia in the sample resulting from an incomplete activation during  
 104        the pre-treatment step for discs prepared at excessively high loads (Figure S7). A similar, but not as  
 105        pronounced, effect has been observed for discs with a lower mass (10 mg).

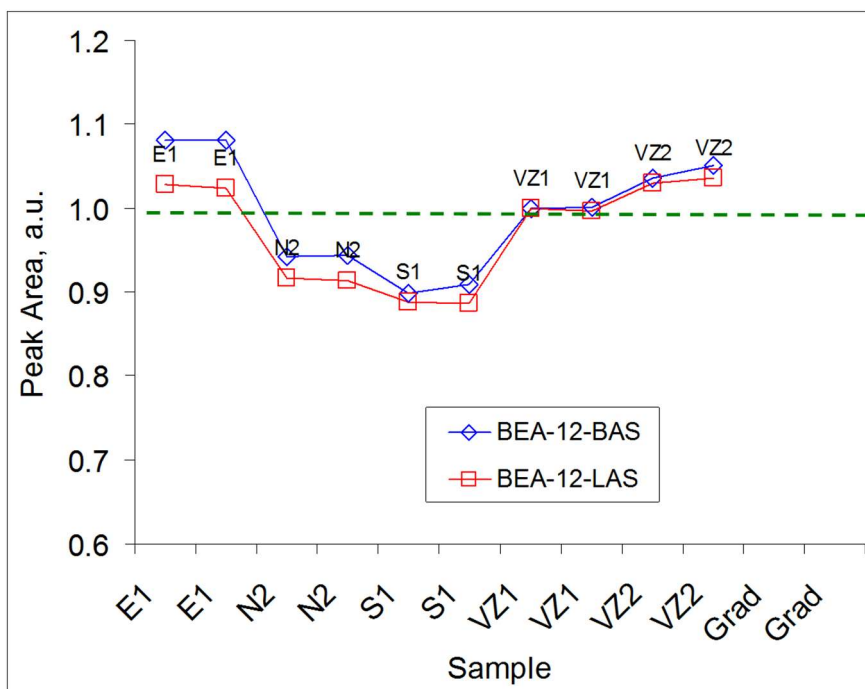


106        **Figure S7.** (a) FTIR spectra of the 40-mg BEA-12 discs prepared under different loads (0.5-8  
 107        tonnes) and activated at 450°C (b) FTIR spectra of the same samples showing the Si-OH-Al peak at  
 108         $\sim 3610 \text{ cm}^{-1}$  (spectra collected at 90°C).

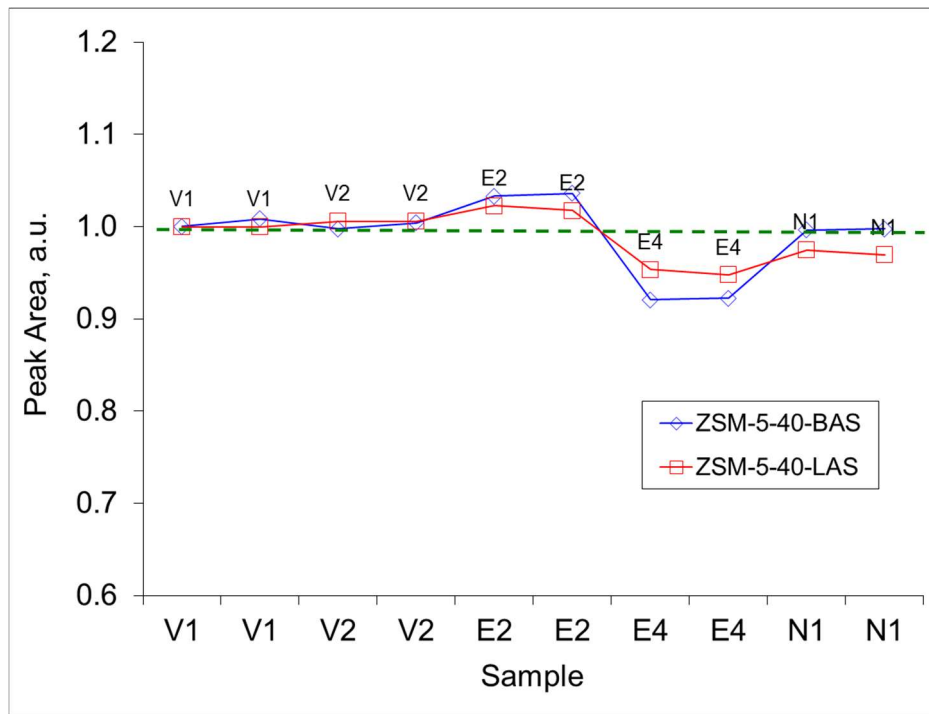
109        *The CARROUCELL experiment.* The results for five ZSM-5-40 and five BEA-12 zeolite  
110        samples are presented in Figures S8-S10 and Table S1.



111  
112        **Figure S8.** The CARROUCELL experiment: FTIR spectra of Py adsorbed on 5 samples of BEA-  
113        12. Two measurements were carried out for each sample (spectra collected at 150°C).  
114



115  
116        **Figure S9.** CARROUCELL experiment: normalised peak areas of Py-B and Py-L complexes on 5  
117        samples of BEA-12. Two measurements were carried out for each sample. The pellets were made  
118        by different experimenters noted E, N, S and V.



121 **Figure S10.** The CARROUCELL experiment: normalised peak areas of Py-B and Py-L complexes  
 122 on 5 samples of ZSM-5-40. Two measurements were carried out for each sample. The pellets were  
 123 made by different experimenters noted E, N, S and V.

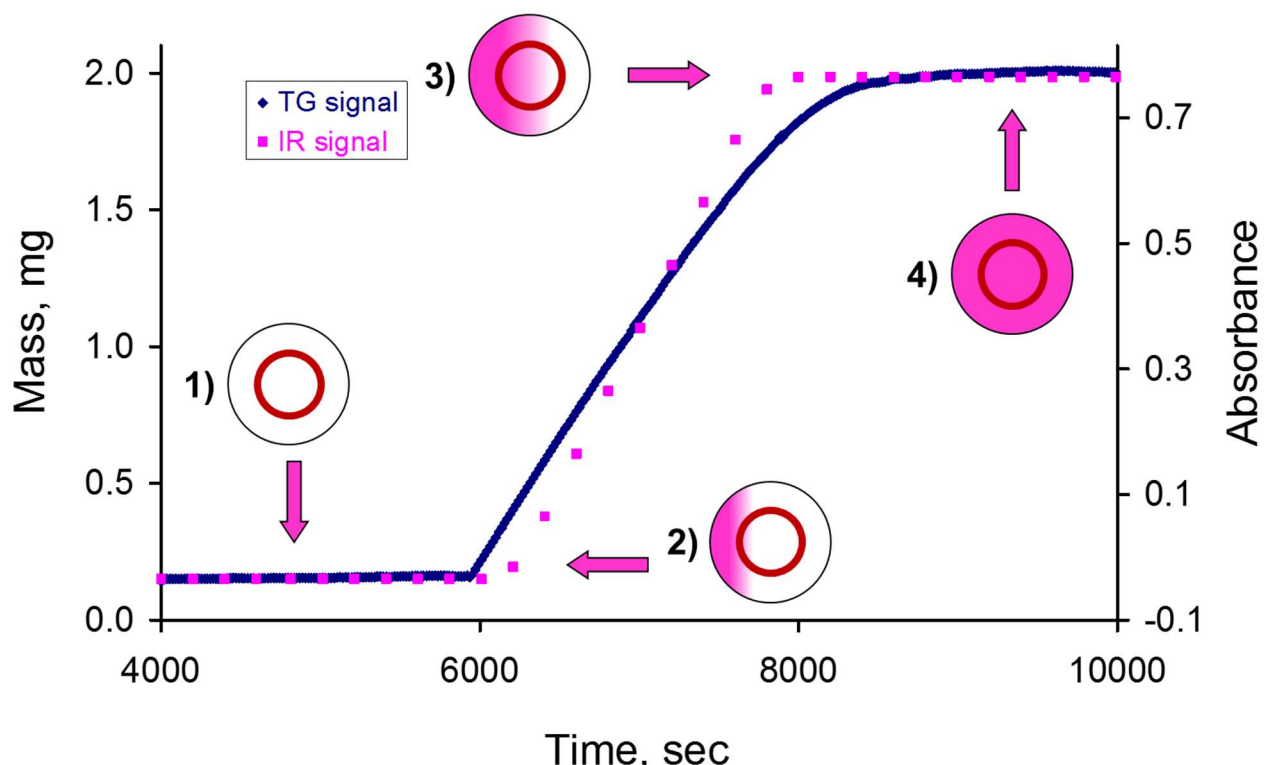
125 **Table S1.** The mean and standard deviation values for the normalised peak areas of Py-B and Py-L  
 126 complexes on ZSM-5-40 and BEA-12 zeolites from the CARROUCELL experiment  
 127 (spectra collected at 150°C).

ZSM-5-40	Py-B ~1545 cm <sup>-1</sup>	Py-L ~1455 cm <sup>-1</sup>
Average	0.992	0.990
STDEVA	0.040	0.027
BEA-12	Py-B	Py-L
Average	0.994	0.972
STDEVA	0.068	0.063

130

*Effect of the cell design.*

131



132

133 **Figure S11.** Schematic representation of Py adsorption on BEA-12: dynamics of the TG and IR  
 134 signals (data collected at 200°C). 1) before Py adsorption, 2) initial stages of Py adsorption, 3)  
 135 final stages of Py adsorption, 4) sample saturated with Py. The red circles show the border of the sample  
 136 area probed by the infrared beam.

137

138

139

140

141      *Effect of the resolution.*

142      The effect of the spectral resolution on both Py-B and Py-L peaks is exemplified using Py  
 143 adsorption at 150°C on BEA-19 (Figure S12). Integration of Py-B and Py-L peaks (Table S2)  
 144 shows that in the spectra collected at 4 cm<sup>-1</sup> there is a significant experimental error when the  
 145 measurements are done by the peak height (~17% for Py-L). To reduce the experimental error, it is  
 146 recommended to use measurements obtained by peak area instead of peak height as the peak area  
 147 measurements are less affected by the resolution.

148

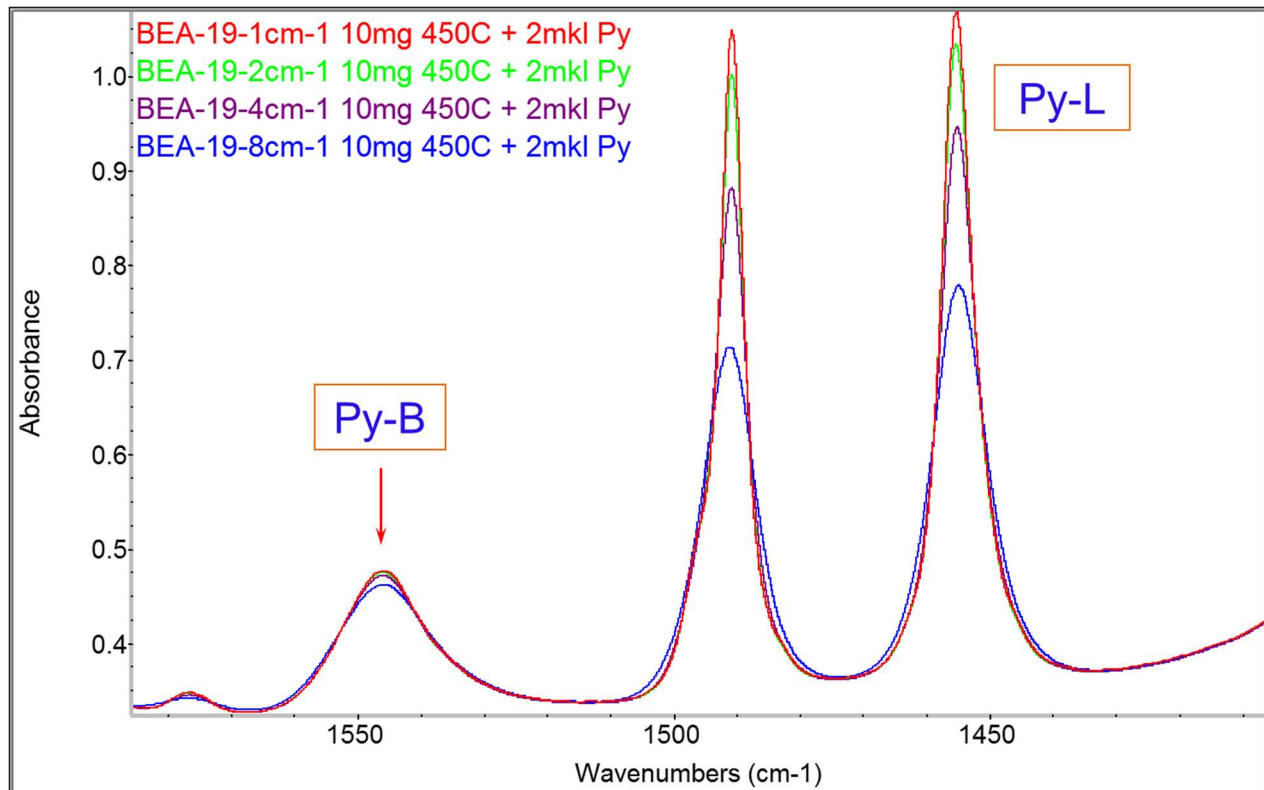


**Figure S12.** FTIR spectra of Py region following Py adsorption at 150°C on BEA-19. Spectra collected at different resolutions, from 1 to 8 cm<sup>-1</sup> (spectra collected at 90°C).

149

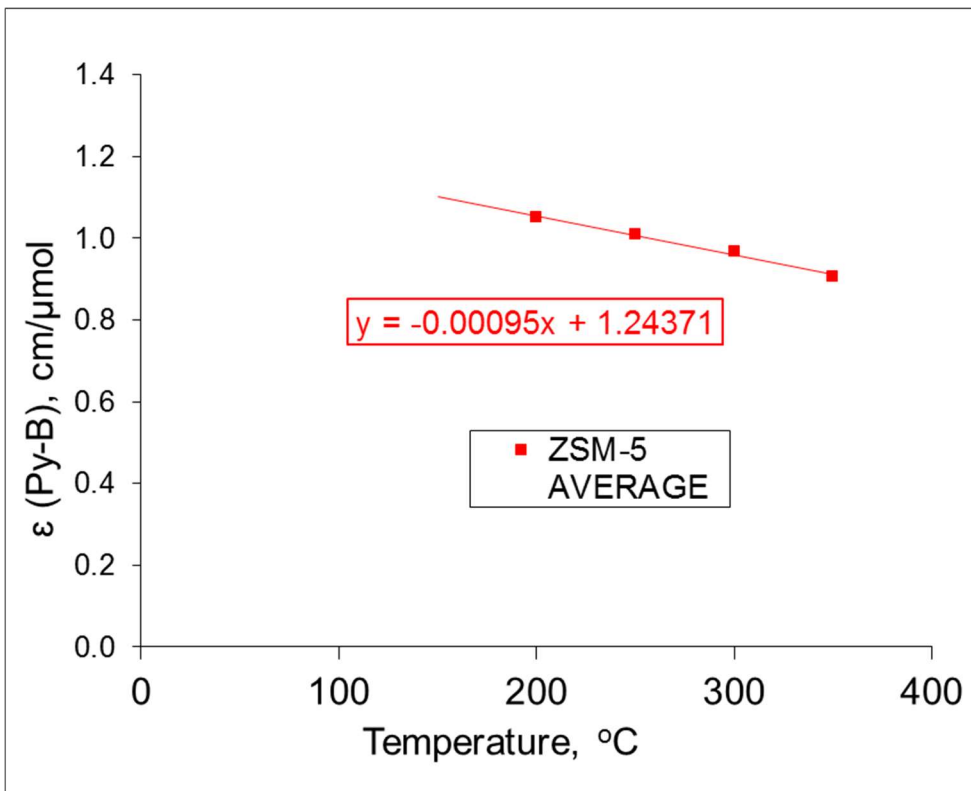
150

151

153 **Table S2.** The peak areas and peak heights of Py-B and Py-L complexes in BEA-19 (at  $\sim$ 1545 and  
 154 at  $\sim$ 1456  $\text{cm}^{-1}$ , respectively) and associated experimental errors (figures **in bold**), taking the spectra  
 155 collected at 1  $\text{cm}^{-1}$  resolution as true value. FWHH is the full width at half-height of the peaks, see  
 156 Figure S12 (spectra collected at 90°C).

Resolution $\text{cm}^{-1}$	FWHH, $\text{cm}^{-1}$		Peak Area, $\text{cm}^{-1}$		Peak height, a.u.	
	Py-B	Py-L	Py-B	Py-L	Py-B	Py-L
1	16.0	6.6	2.52	5.40	0.15	0.70
			-	-	-	-
2	16.2	6.8	2.51	5.30	0.14	0.67
			<b>0.6%</b>	<b>1.9%</b>	<b>0.7%</b>	<b>4.7%</b>
4	16.6	7.8	2.50	5.08	0.14	0.58
			<b>0.6%</b>	<b>5.9%</b>	<b>2.8%</b>	<b>17.1%</b>
8	18.0	10.7	2.43	4.63	0.13	0.41
			<b>3.5%</b>	<b>14.3%</b>	<b>10.3%</b>	<b>41.3%</b>

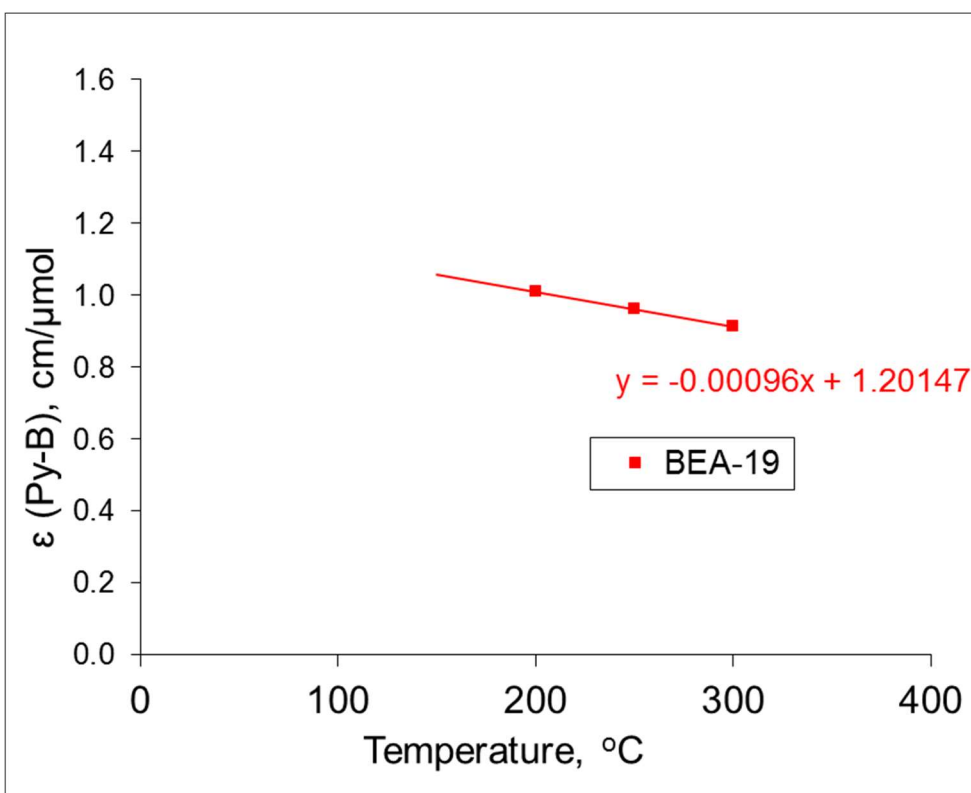
161 *Effect of the temperature*



162

163 **Figure S13a.** The mean integrated molar absorption coefficient of Py-B complexes for ZSM-5  
164 samples as a function of the temperature of the FTIR measurements.

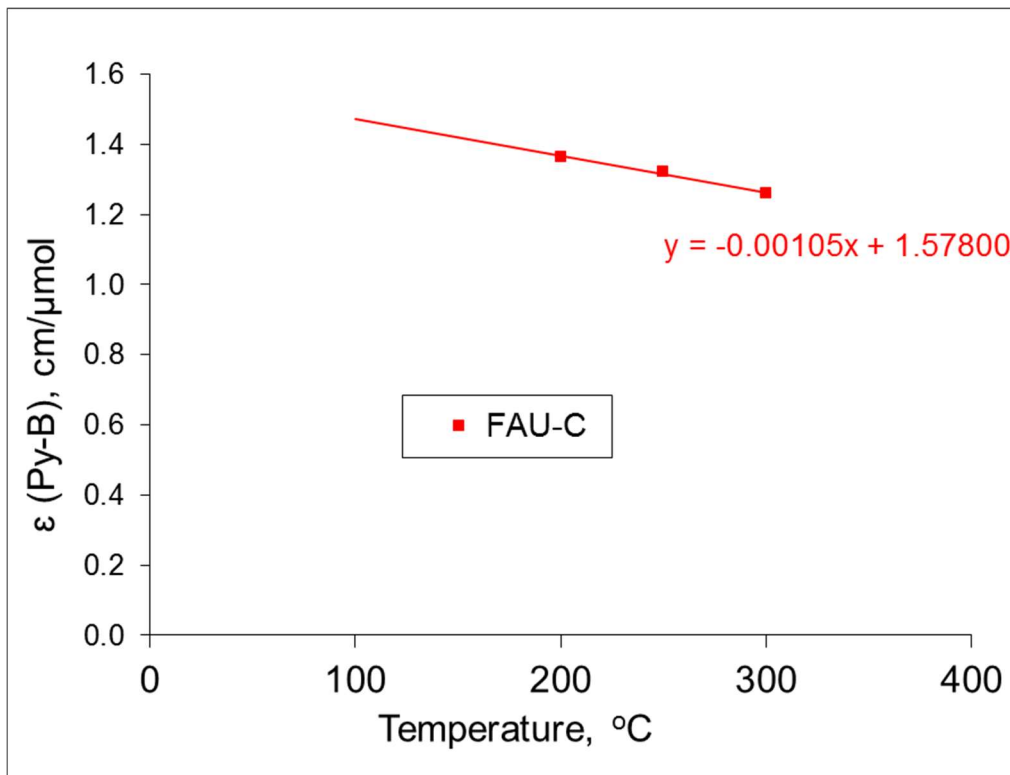
165



166

167 **Figure S13b.** The integrated molar absorption coefficients of Py-B complexes for BEA-19 as a  
168 function of the temperature of the FTIR measurements.

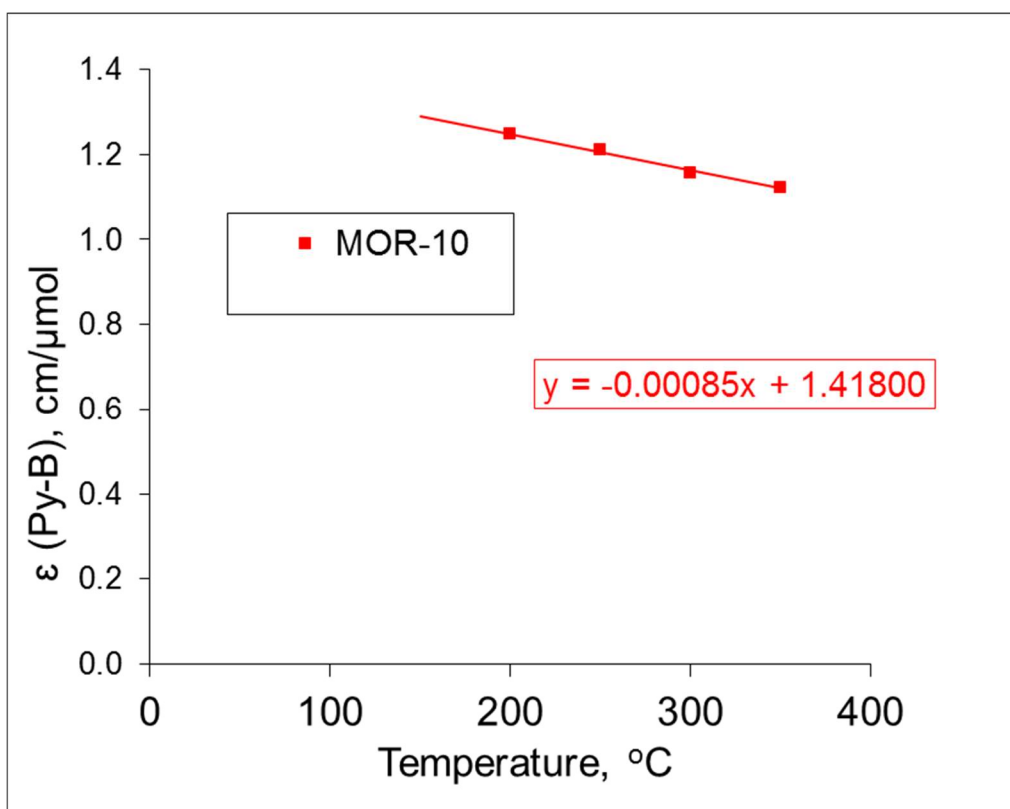
169



170

Figure S13c. The integrated molar absorption coefficient of Py-B complexes for FAU-C as a function of the temperature of the FTIR measurements.

173



174

Figure S13d. The integrated molar absorption coefficient of Py-B complexes for MOR-10 as a function of the temperature of the FTIR measurements.

177

178 **Table S3.** Statistical data ( $\epsilon$ (Py-B) values, units = cm/ $\mu$ mol), produced via repeated measurements  
 179 on different zeolite samples, for the integrated molar absorption coefficients of Py-B complexes  
 180 obtained by AGIR measurements at 200-350°C.

181

Sample		ZSM-5	ZSM-5	ZSM-5	ZSM-5	BEA-19	FAU-C
Temp, °C		200	250	300	350	200	200
$\epsilon$ (Py-B)	ZSM-5-40	1.044	0.993	0.931	0.905	0.940	1.36
cm/ $\mu$ mol	ZSM-5-40	1.003	0.956	0.907	0.874	1.100	1.54
	ZSM-5-40	1.092	1.046	0.983	0.961	1.080	1.41
	ZSM-5-40	1.035	0.980	0.936	0.885	1.010	1.5
	ZSM-5-40	1.017	0.964	0.900		1.140	1.51
	ZSM-5-40	1.091	1.020	1.021		1.150	
	ZSM-5-40-600°C	1.064	1.085	1.067			
	ZSM-5-40-700°C	1.084	1.044	1.000			
	ZSM-5-27	1.045	1.021	0.991			
	ZSM-5-27	1.029	0.977	0.949			
<b>AVERAGE</b>		<b>1.051</b>	<b>1.009</b>	<b>0.968</b>	<b>0.906</b>	<b>1.070</b>	<b>1.464</b>
<b>STDEVA</b>		<b>0.031</b>	<b>0.042</b>	<b>0.053</b>	<b>0.039</b>	<b>0.081</b>	<b>0.076</b>

182

183

184  
185**Table S4.** Statistical data for the peak positions of Py-B and Py-L complexes and of OH-groups (in cm<sup>-1</sup>) on various zeolites obtained from AGIR measurements at 200-300°C.

Sample	ZSM-5-40	ZSM-5-40	ZSM-5-40	BEA-19	BEA-19	BEA-19	Sample	FAU-C	FAU-C	FAU-C	US-Y	US-Y	US-Y	MOR-10	MOR-10	MOR-10
Temp, oC	200	250	300	200	250	300	Temp, oC	200	250	300	200	250	300	200	250	300
<b>Peak</b>	1544.5	1543.4	1542.4	1544.0	1543.0	1542.3	<b>Peak</b>	1540.6	1540.0	1539.1				1542.8	1541.7	1540.7
<b>Py-B</b>	1544.1	1543.2	1542.3	1543.3	1542.8	1541.7	<b>Py-B</b>	1540.9	1540.2	1539.4				1542.9	1541.8	1540.8
cm-1	1544.5	1543.8	1542.8	1543.9	1543.0	1542.2	cm-1				1543.1	1542.3	1541.5			
	1544.2	1543.3	1542.5	1543.6	1542.6	1541.7					1542.3	1541.6	1541.0			
	1544.1	1543.3	1542.5													
	1544.2	1543.1	1542.1													
<b>AVERAGE</b>	1544.3	1543.4	1542.4	1543.7	1542.9	1542.0	<b>AVERAGE</b>	1540.8	1540.1	1539.3	1542.7	1542.0	1541.3	1542.9	1541.8	1540.8
<b>STDEVA</b>	0.19	0.24	0.23	0.32	0.19	0.32	<b>STDEVA</b>	0.21	0.14	0.21	0.57	0.49	0.35	0.07	0.07	0.07
Sample	ZSM-5-40	ZSM-5-40	ZSM-5-40	BEA-19	BEA-19	BEA-19	Sample	FAU-C	FAU-C	FAU-C	US-Y	US-Y	US-Y	MOR-10	MOR-10	MOR-10
Temp, oC	200	250	300	200	250	300	Temp, oC	200	250	300	200	250	300	200	250	300
<b>Peak</b>	1454.9	1454.6	1454.3	1454.7	1454.4	1453.9	<b>Peak</b>	1453.8	1453.5	1453.2				1454.0	1453.6	1453.2
<b>Py-L</b>	1454.6	1454.4	1454.2	1454.5	1454.1	1453.7	<b>Py-L</b>	1452.9	1452.4	1452.0				1453.9	1453.5	1453.0
cm-1	1455.1	1454.7	1454.3	1454.3	1453.9	1453.5	cm-1				1454.6	1454.3	1453.9			
	1455.7	1455.4	1454.8	1455.1	1454.7	1454.2					1454.1	1453.5	1453.1			
	1455.6	1454.9	1454.6													
	1455.9	1455.2	1454.6													
<b>AVERAGE</b>	1455.3	1454.9	1454.5	1454.7	1454.3	1453.8	<b>AVERAGE</b>	1453.4	1453.0	1452.6	1454.4	1453.9	1453.5	1454.0	1453.6	1453.1
<b>STDEVA</b>	0.51	0.38	0.23	0.34	0.35	0.30	<b>STDEVA</b>	0.64	0.78	0.85	0.35	0.57	0.57	0.07	0.07	0.14
Al(OH)Si LF								3546.3	3545.8	3545.1						
Al(OH)Si HF	3603.4	3601.3	3598.9	3605.0	3603.4	3601.3		3636.4	3634.6	3632.5				3603.1	3600.4	3597.6
SiOH	3738.1	3736.9	3735.6	3733.8	3732.9	3732.0		3742.1	3741.2	3740.2				3742.7	3741.8	3740.7

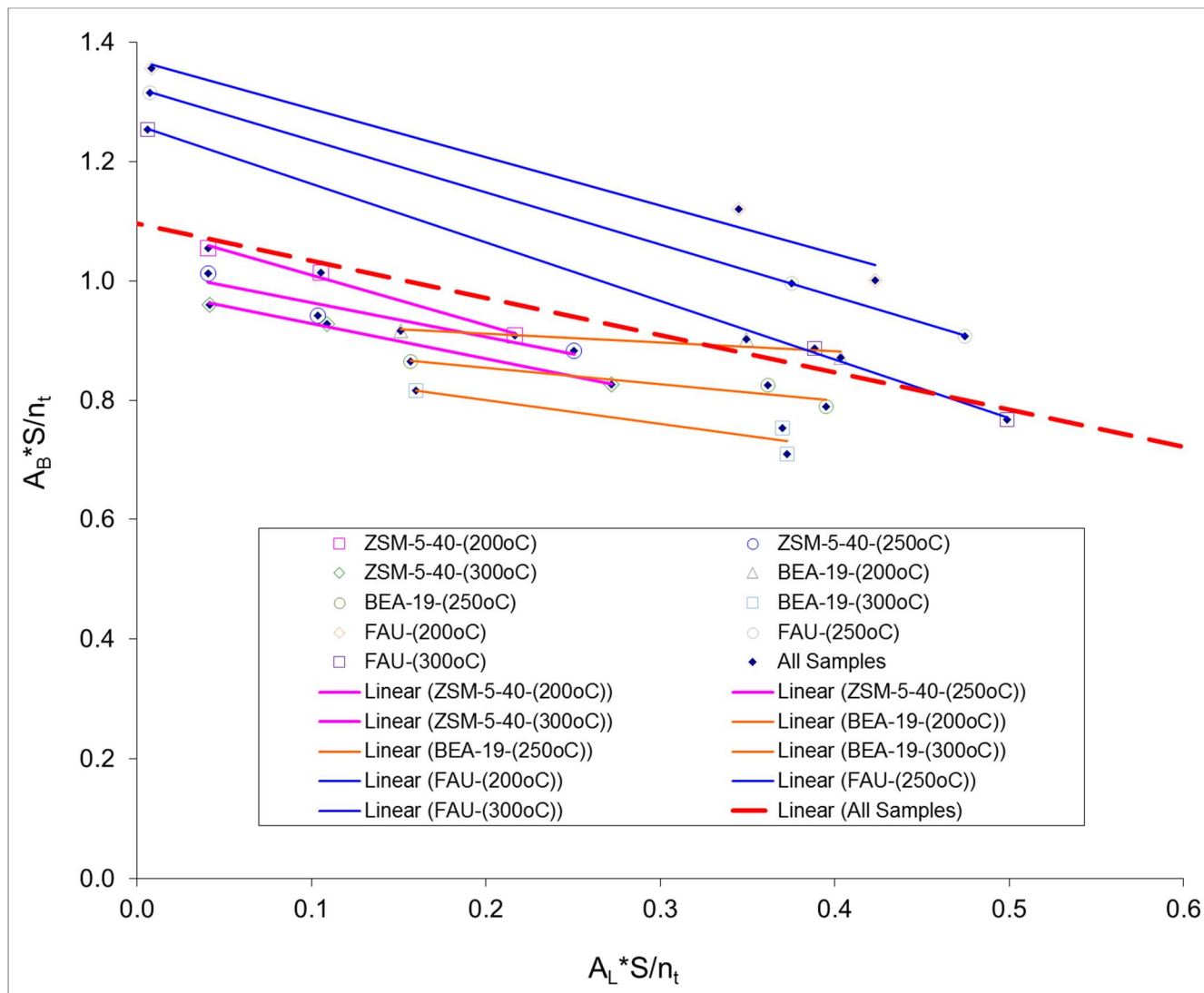
186

187

188    *Experimental data for the samples containing both BAS and LAS.*189       By using the following equation, both  $\epsilon(\text{Py-B})$  and  $\epsilon(\text{Py-L})$  values have been determined from  
190       the gradient and the y-intercept of the trend lines.

191       
$$\frac{A_B \times S}{n_{total}} = -\frac{\epsilon_B}{\epsilon_L} \times \frac{A_L \times S}{n_{total}} + \epsilon_B$$

192



193

194       **Figure S14.** Characterisation of ZSM-5-40, BEA-19 and faujasite zeolite samples containing both  
195       Py-B and Py-L complexes. The temperature values in brackets indicate the temperature of the FTIR  
196       measurements.

197

198

199

200 **Table S5.** Statistical data, produced via repeated measurements, for the integrated molar absorption  
201 coefficients of Py-B and Py-L complexes on various zeolite samples with different ratio of  
202 BAS/LAS, obtained by AGIR measurements at 200°C ( $\epsilon$ (Py-B) and  $\epsilon$ (Py-L) values, units =  
203 cm/ $\mu$ mol).

204

Sample	ZSM-5-40		BEA-19		FAU	
	$\epsilon$ (Py-B)	$\epsilon$ (Py-L)	$\epsilon$ (Py-B)	$\epsilon$ (Py-L)	$\epsilon$ (Py-B)	$\epsilon$ (Py-L)
	1.06	1.66	0.94	6.38	1.41	1.72
	1.06	1.68	1.10	1.92	1.37	1.69
	1.07	1.51			1.41	1.73
	1.08	1.72				
Average	<b>1.07</b>	<b>1.64</b>	<b>1.02</b>	<b>4.15</b>	<b>1.39</b>	<b>1.71</b>
STDEVA	0.01	0.09	0.11	3.15	0.02	0.02

205

206

207

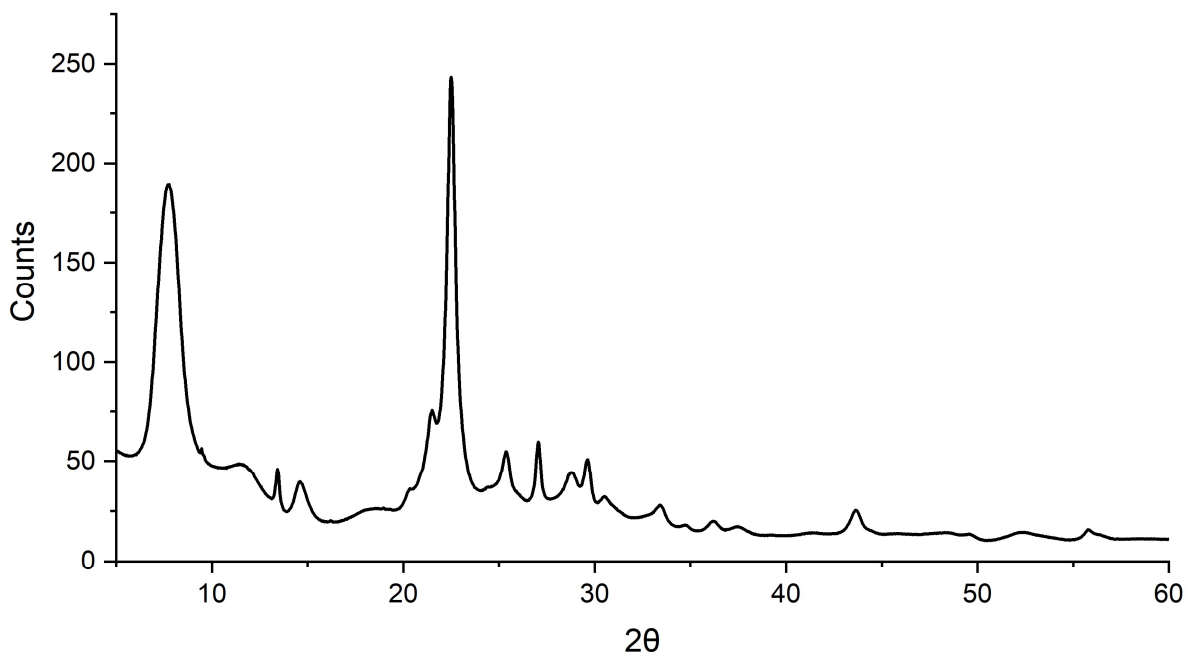
208

209

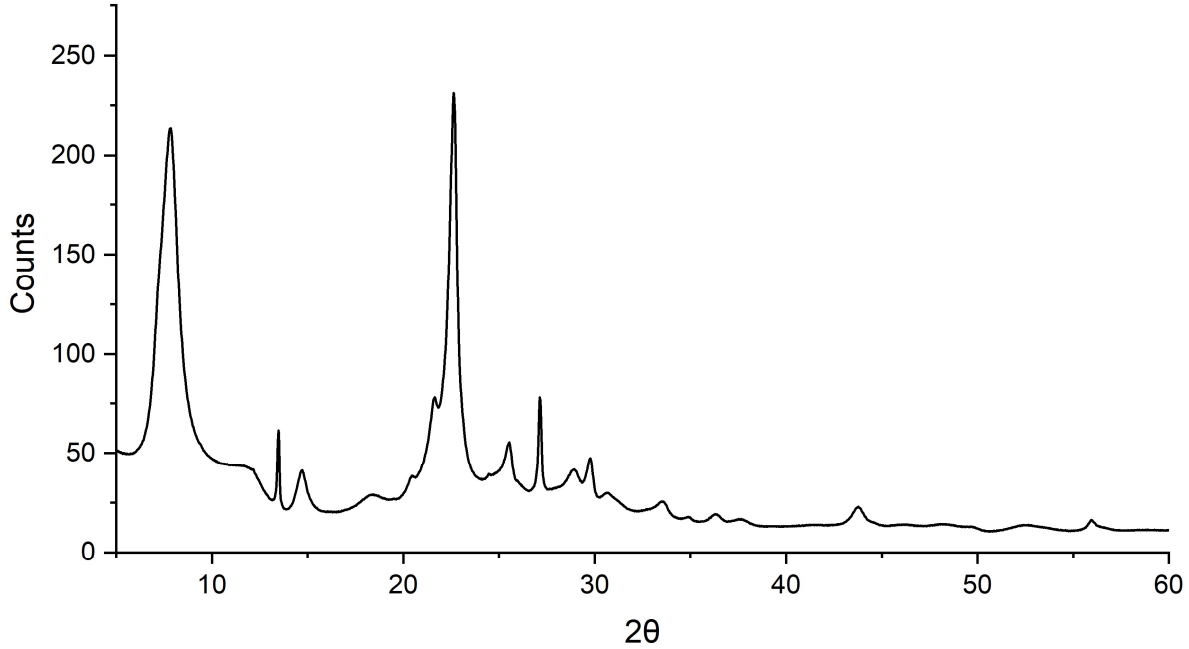
210  
211  
212

## Appendix: Characterisation data for the samples studied in this work

### XRD data

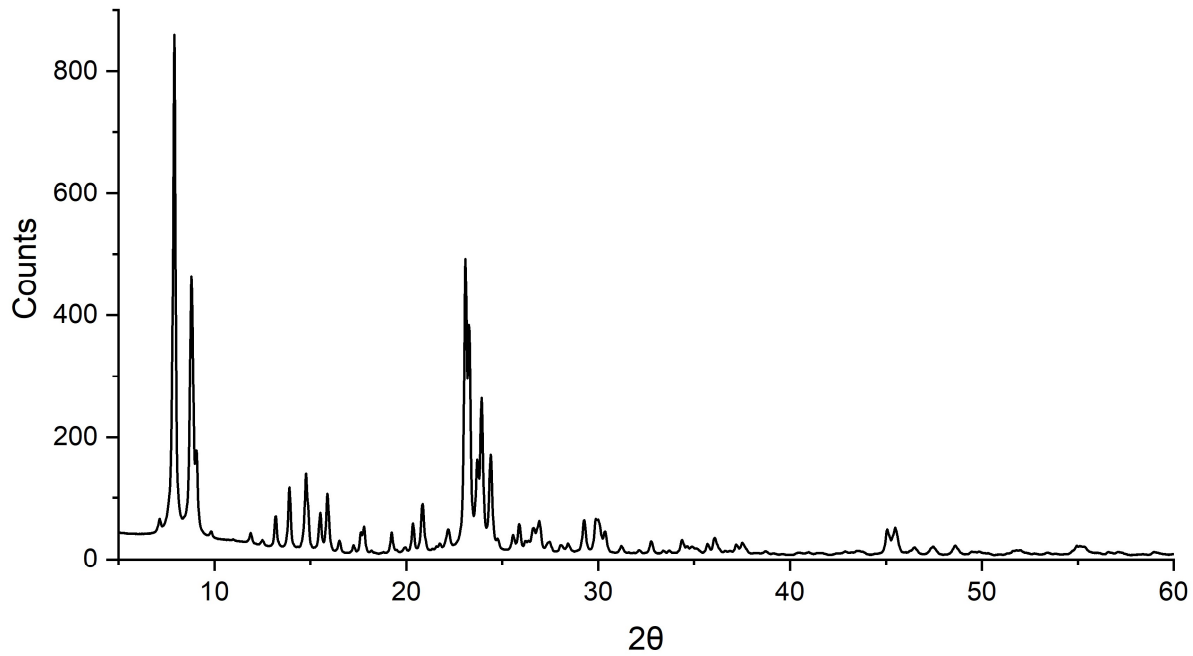


**Figure S15a.** XRD pattern of BEA-12.

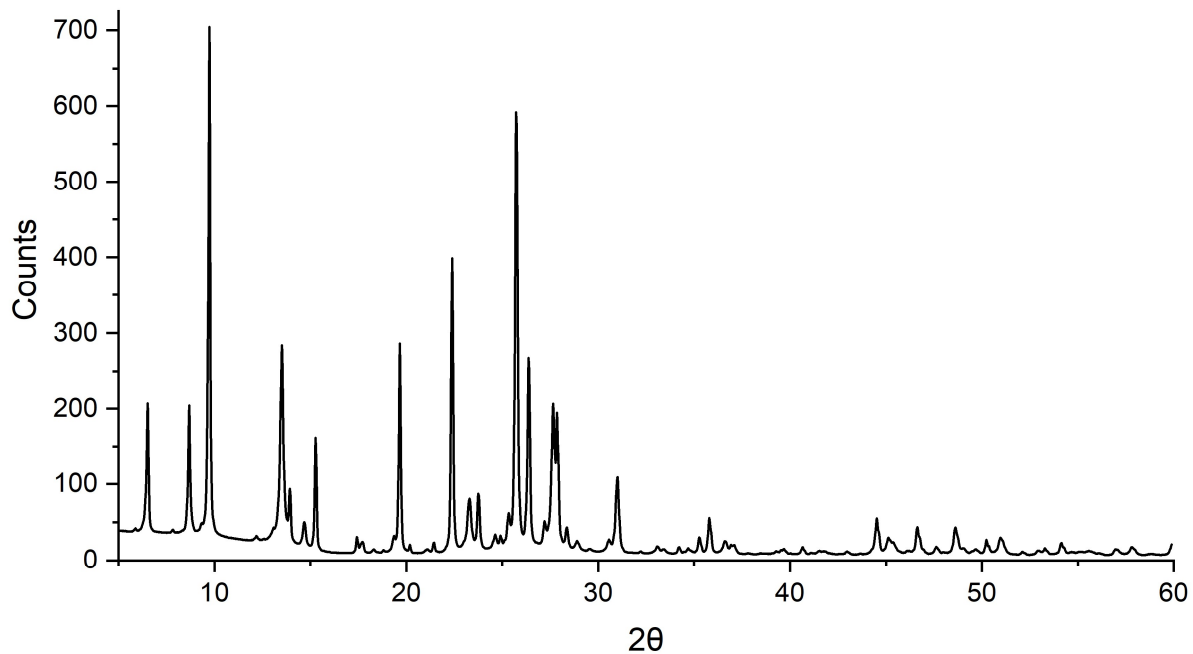


**Figure S15b.** XRD pattern of BEA-19.

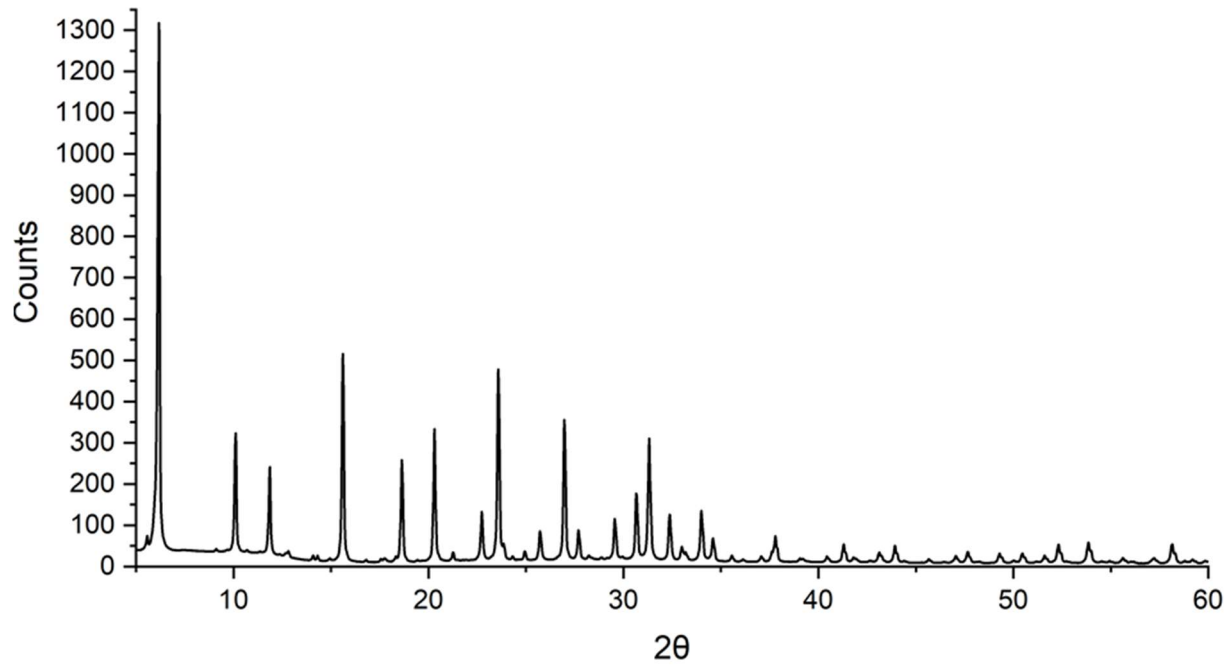
213  
214



**Figure S15c.** XRD pattern of ZSM-5-40.



**Figure S15d.** XRD pattern of MOR-10.

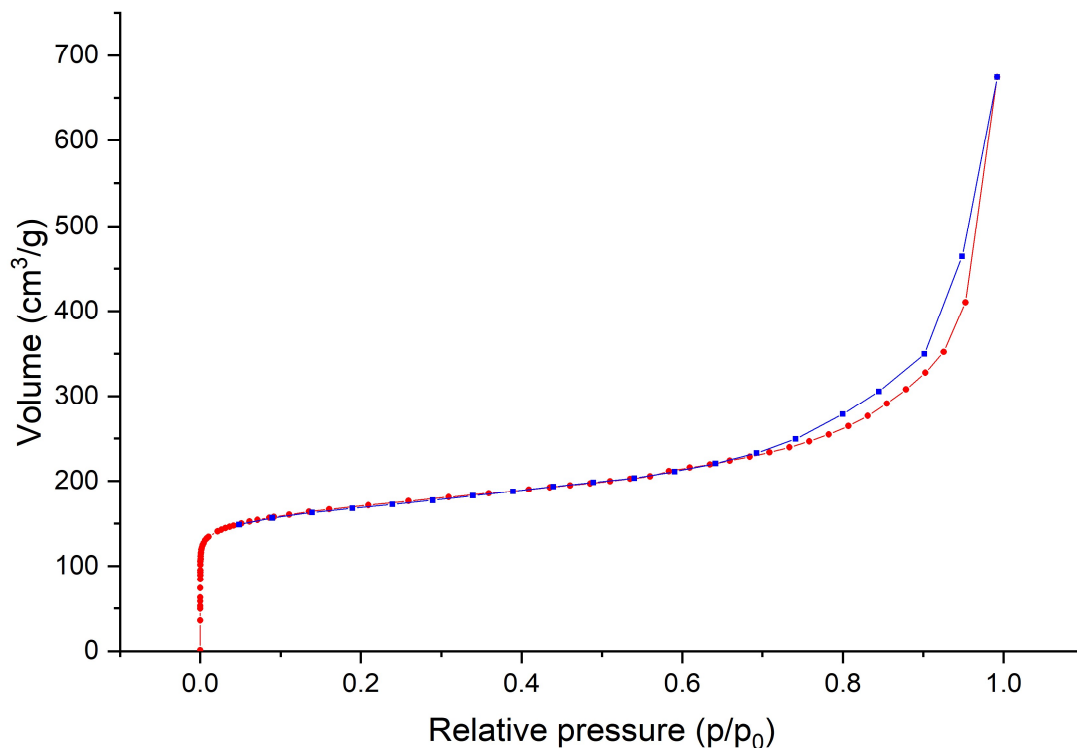
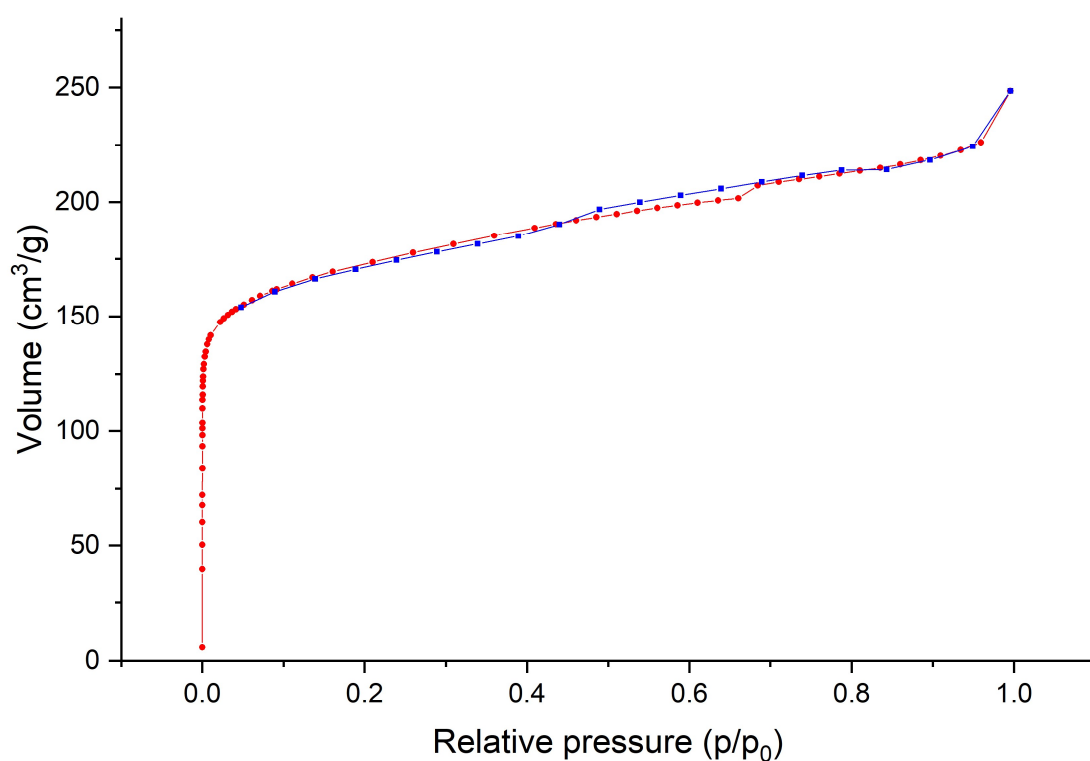


**Figure S15e.** XRD pattern of FAU-C.

216

217

218

**Nitrogen adsorption data****Figure S16a.** Nitrogen adsorption-desorption isotherm for BEA-12.**Figure S16b.** Nitrogen adsorption-desorption isotherm for BEA-19.

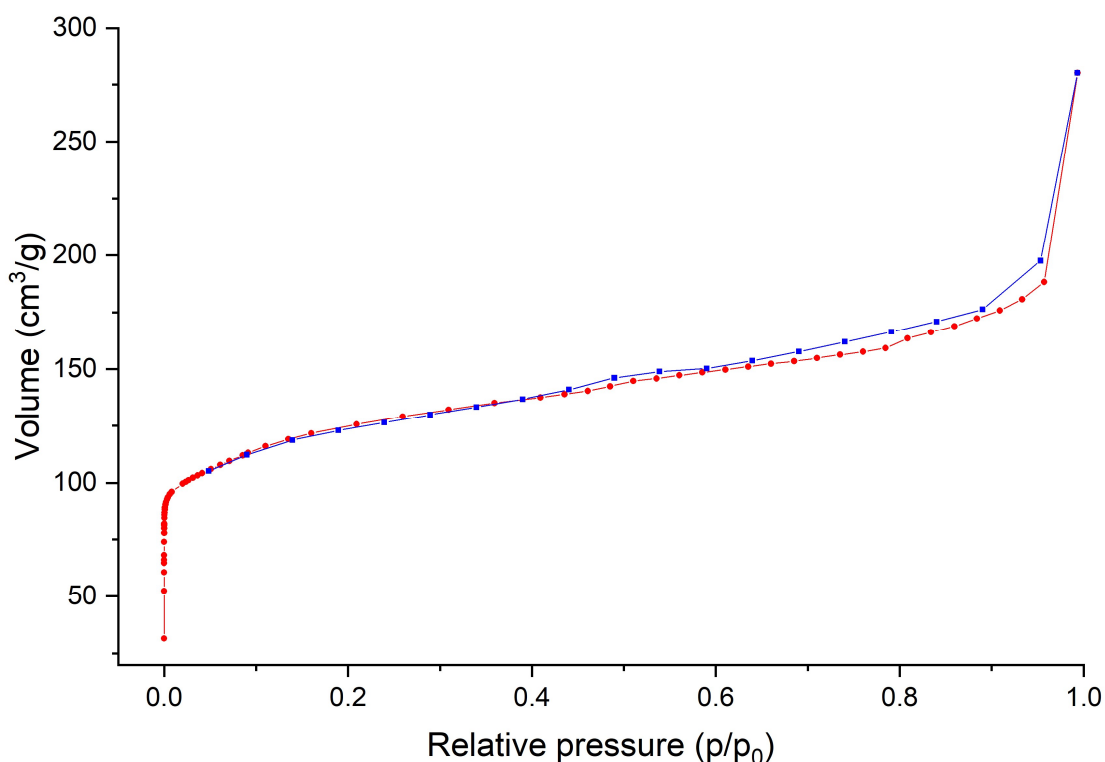


**Figure S16c.** Nitrogen adsorption-desorption isotherm for ZSM-5-40.

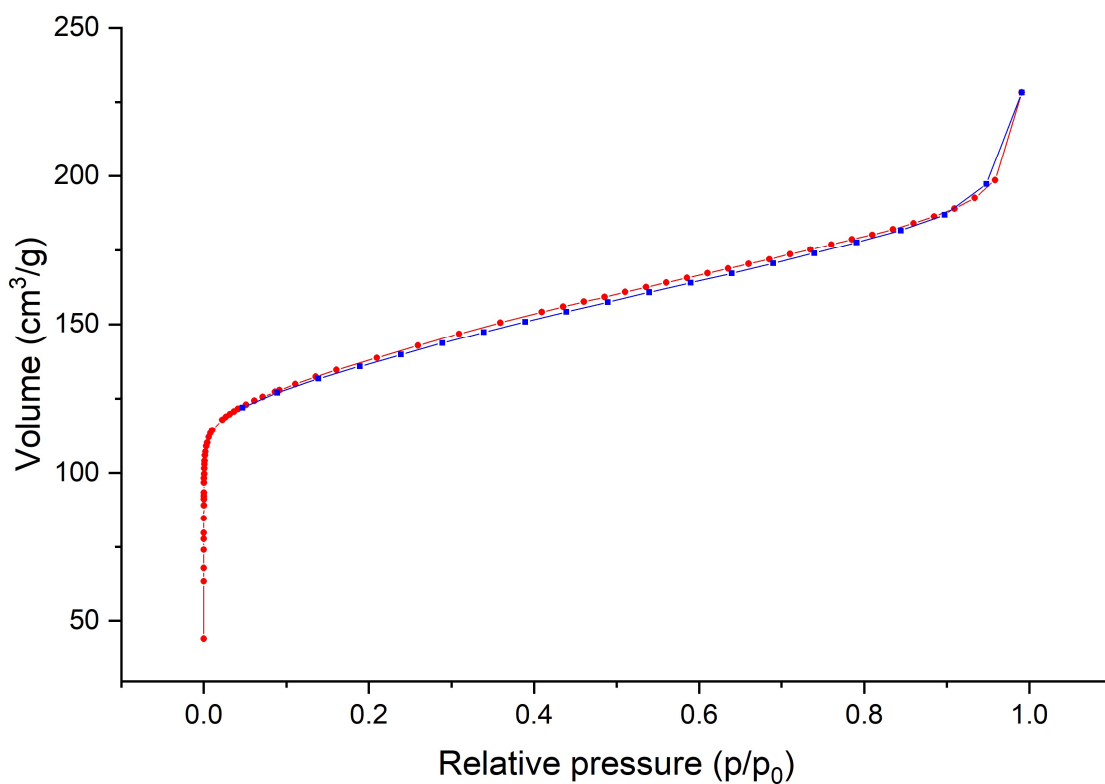
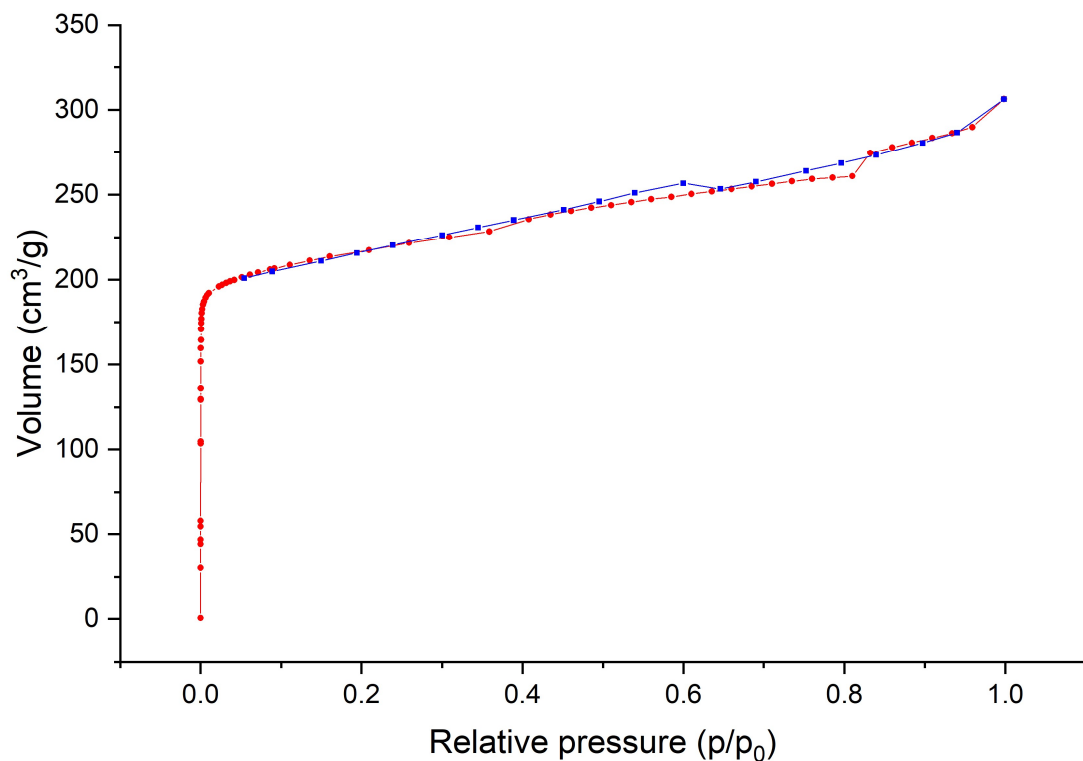


**Figure S16d.** Nitrogen adsorption-desorption isotherm for MOR-10.



220 **Figure S16e.** Nitrogen adsorption-desorption isotherm for FAU-Z.

221

222

223

**TGA data**

224

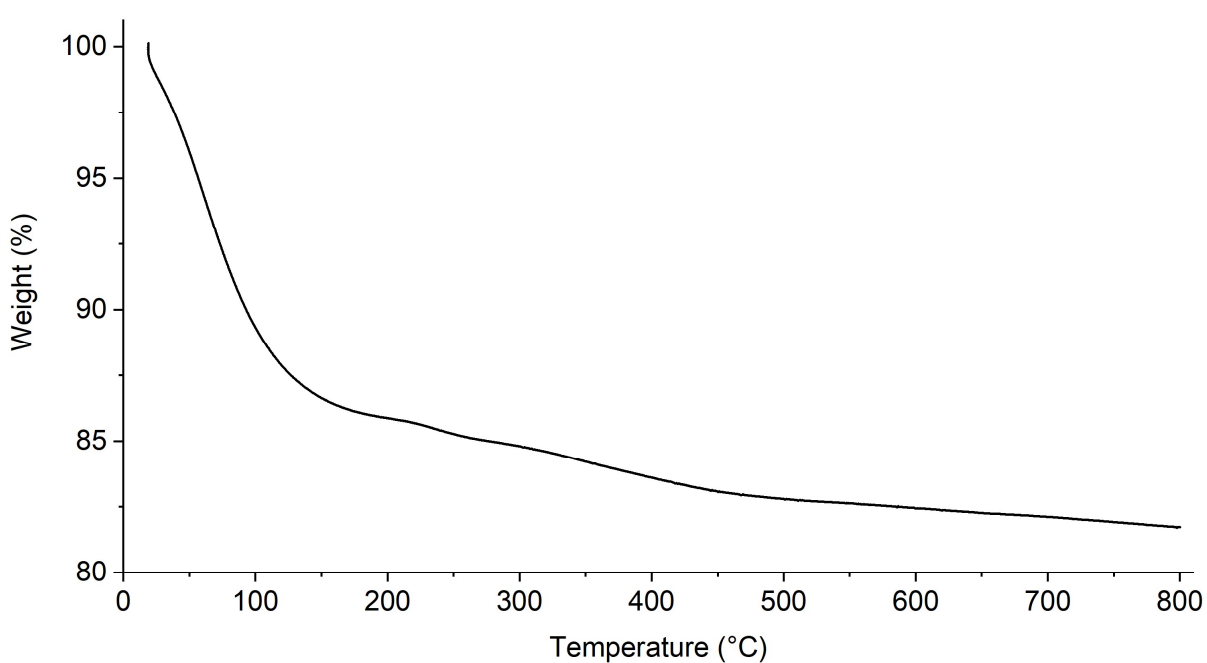


**Figure S17a.** Thermogravimetric analysis curve of BEA-12.

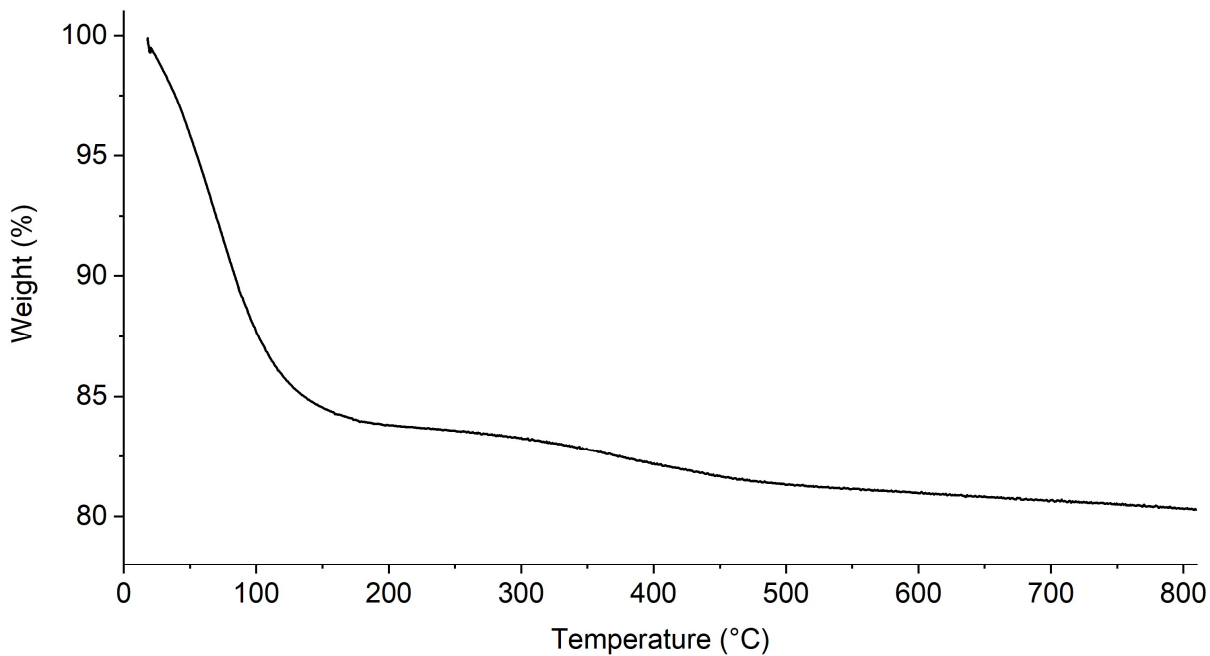


**Figure S17b.** Thermogravimetric analysis curve of BEA-19.

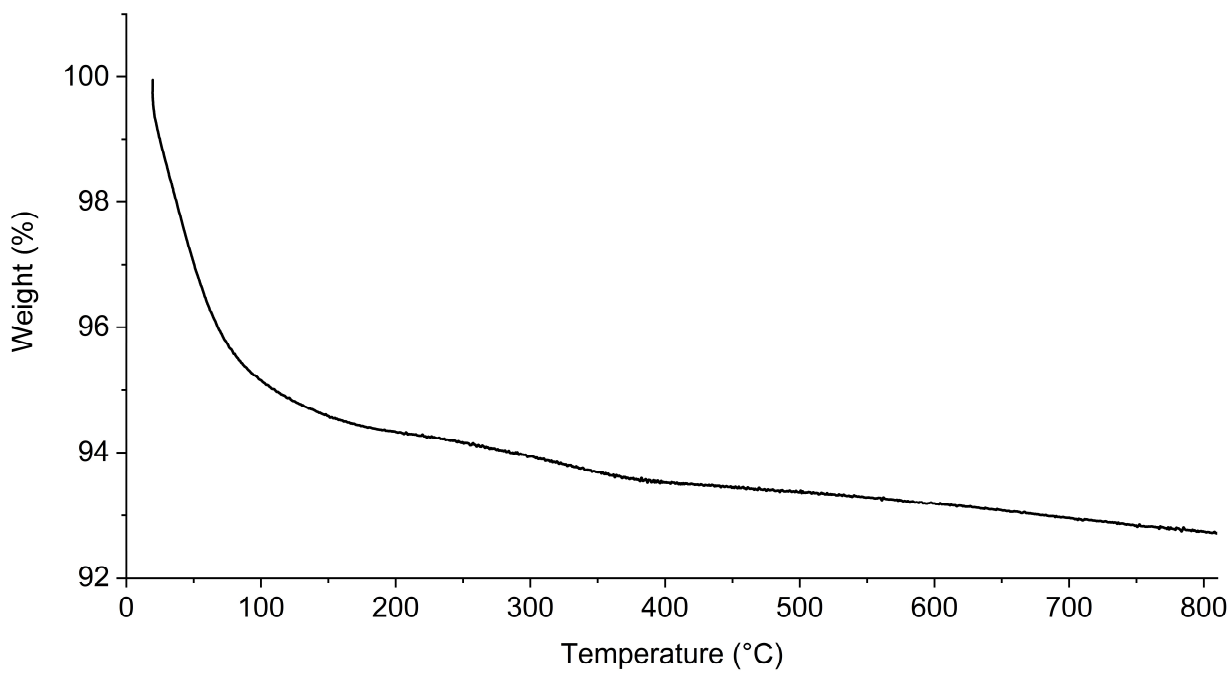


**Figure S17c.** Thermogravimetric analysis curve of ZSM-5-40.

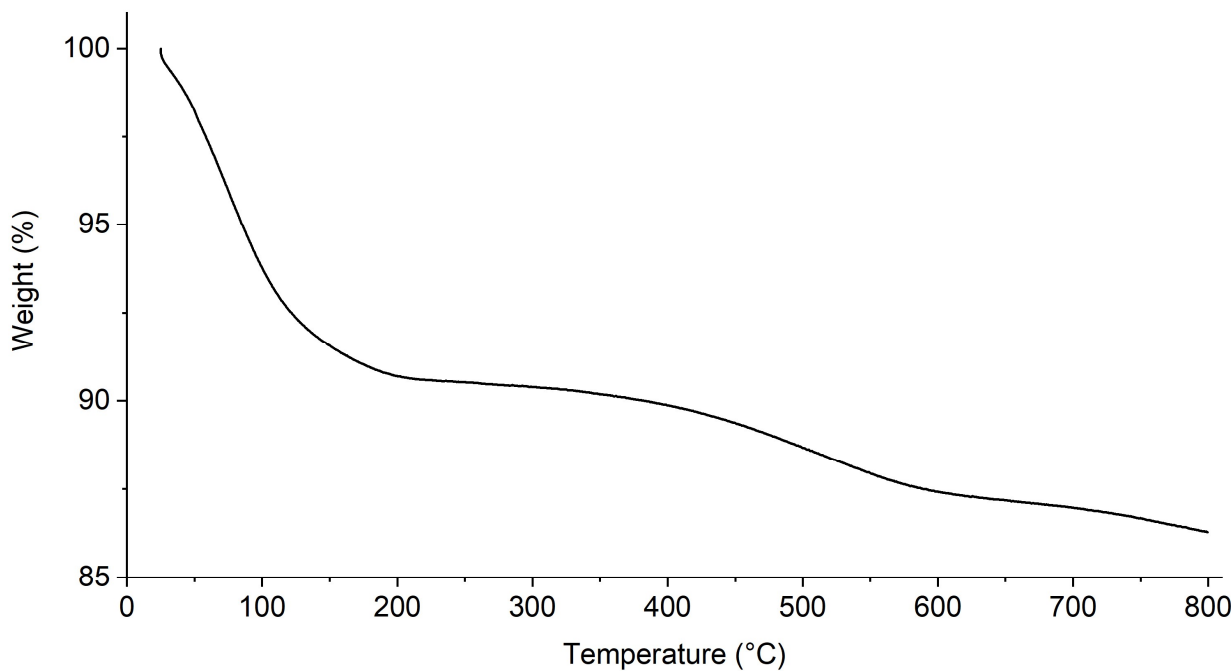


**Figure S17d.** Thermogravimetric analysis curve of MOR-10.

225

226

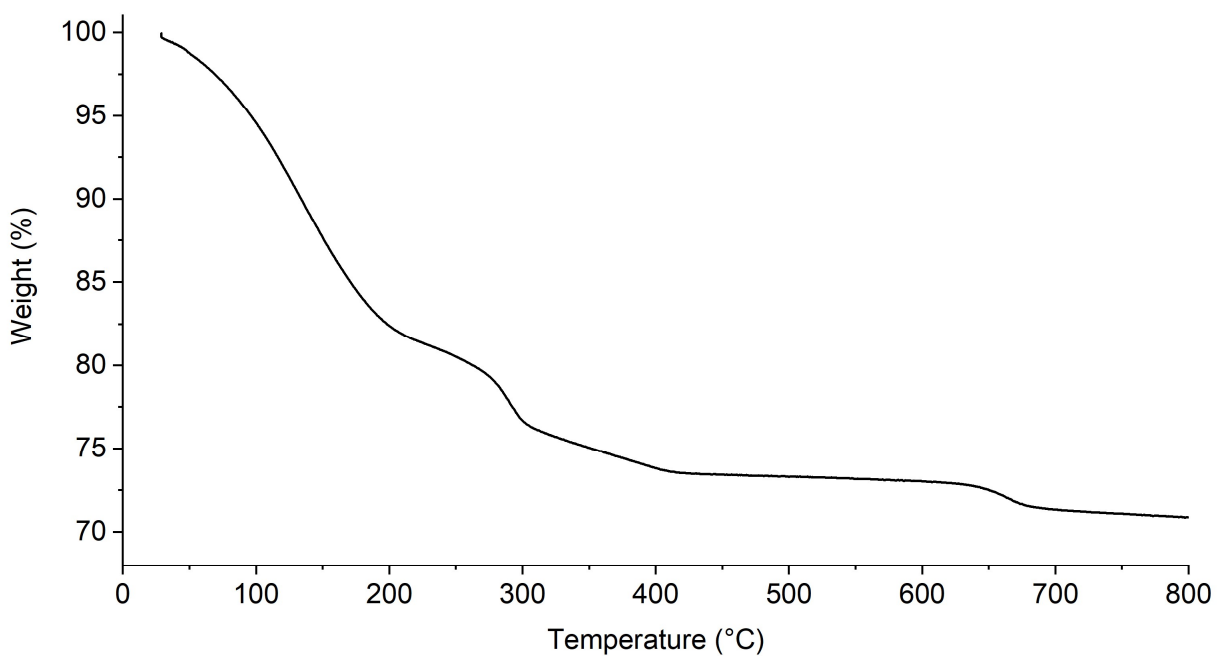


**Figure S17f.** Thermogravimetric analysis curve of FAU-Z.

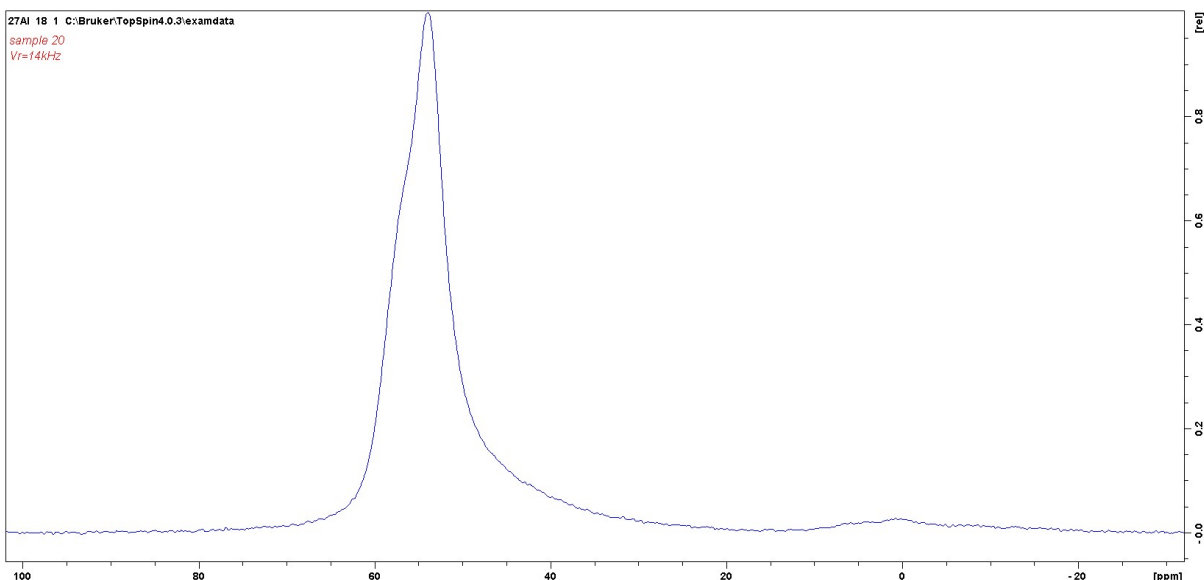
227

228

229

## NMR data

230

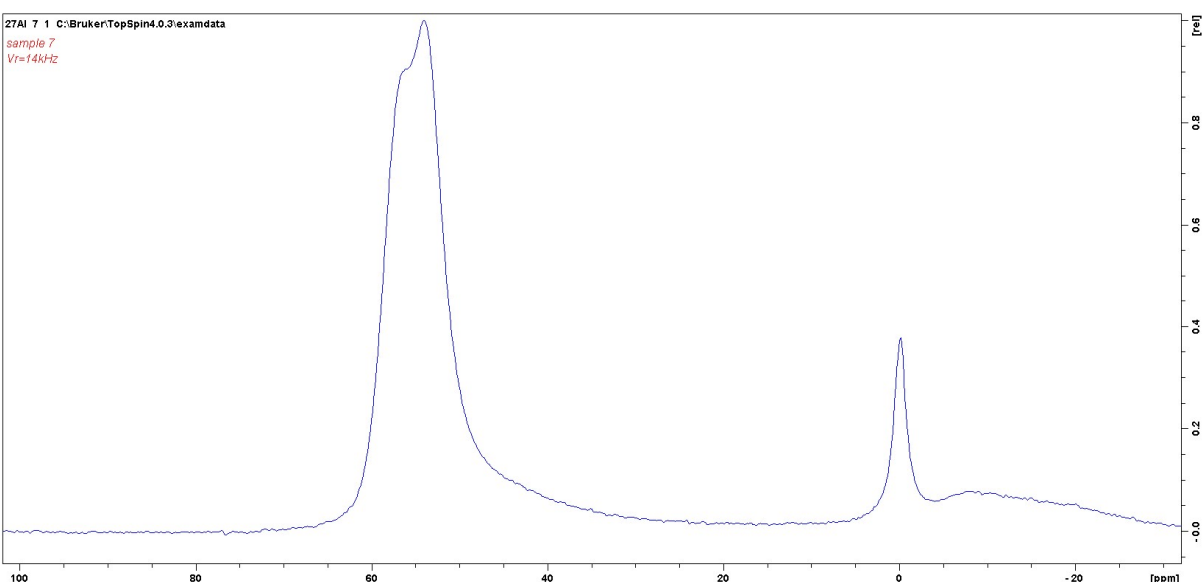


231

**FigureS18a.** <sup>27</sup>Al-NMR spectrum of BEA-12.

233

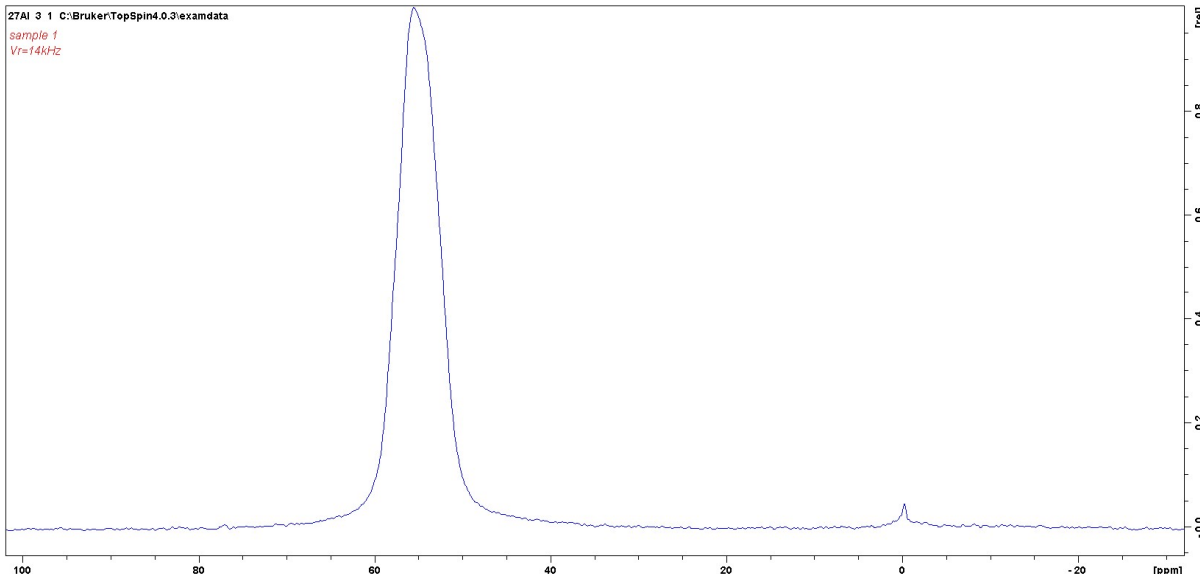
234



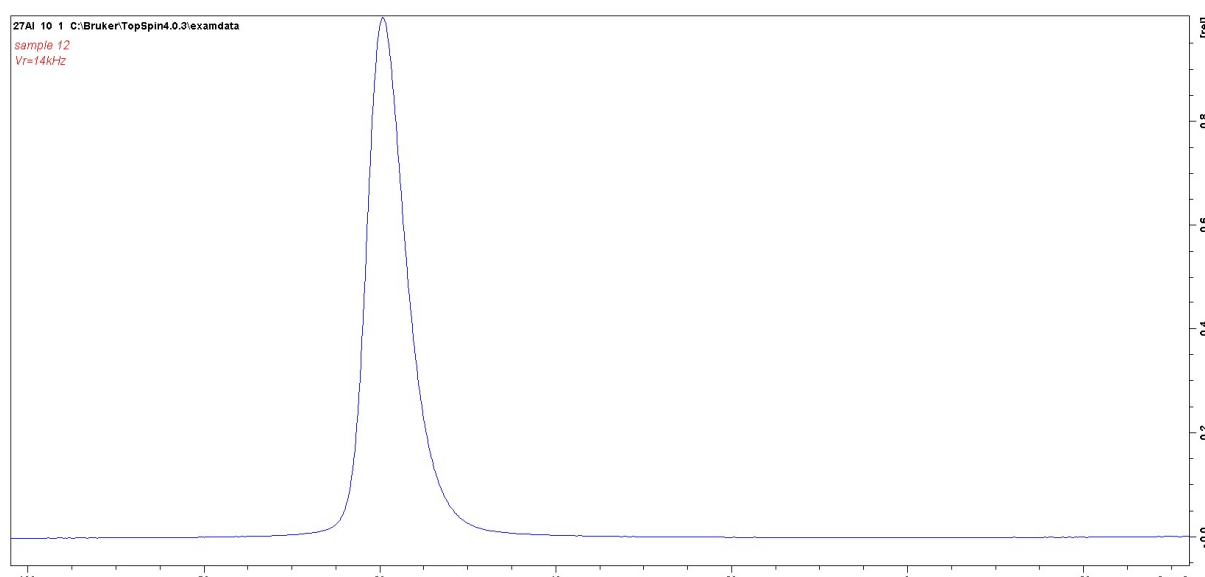
235

**FigureS18b.** <sup>27</sup>Al-NMR spectrum of BEA-19.

237

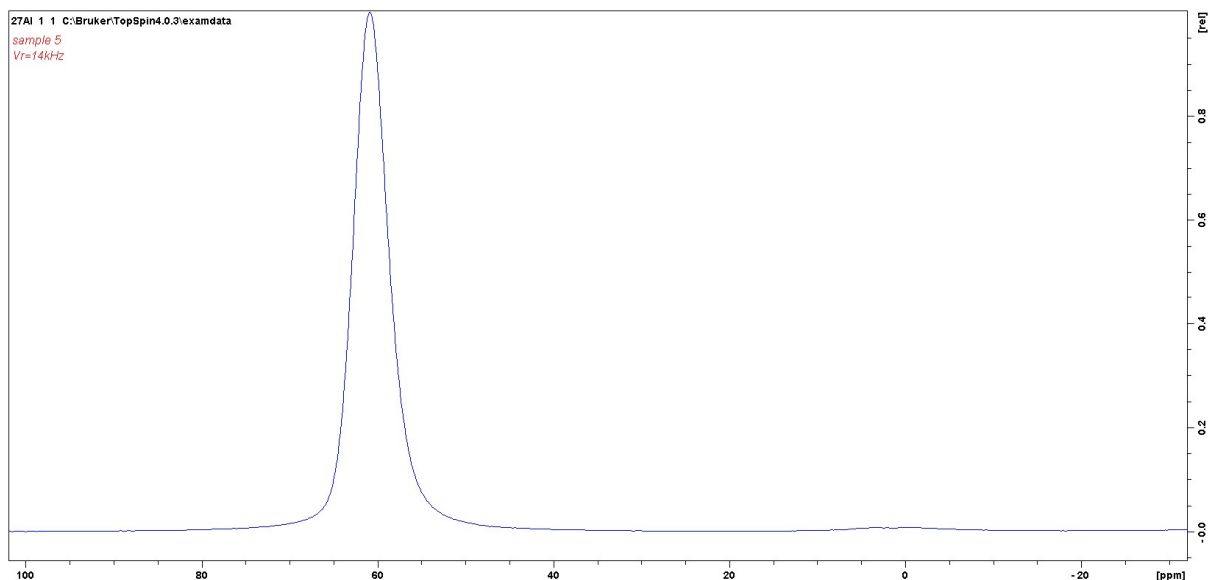


**FigureS18c.**  $^{27}\text{Al}$ -NMR spectrum of ZSM-5-40.



**FigureS18d.**  $^{27}\text{Al}$ -NMR spectrum of MOR-10.

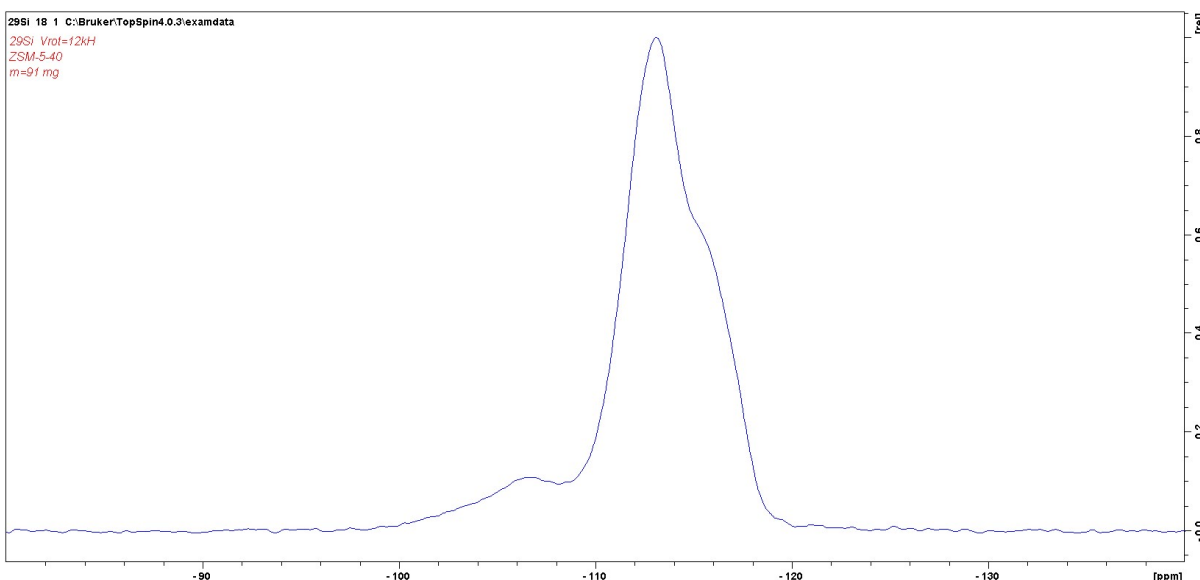
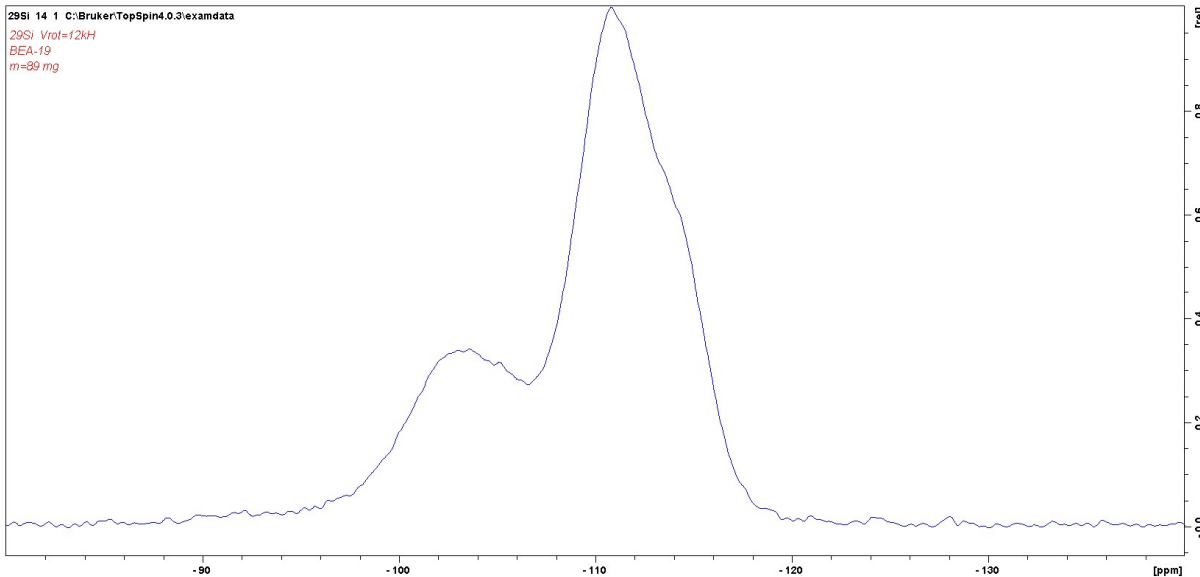
245

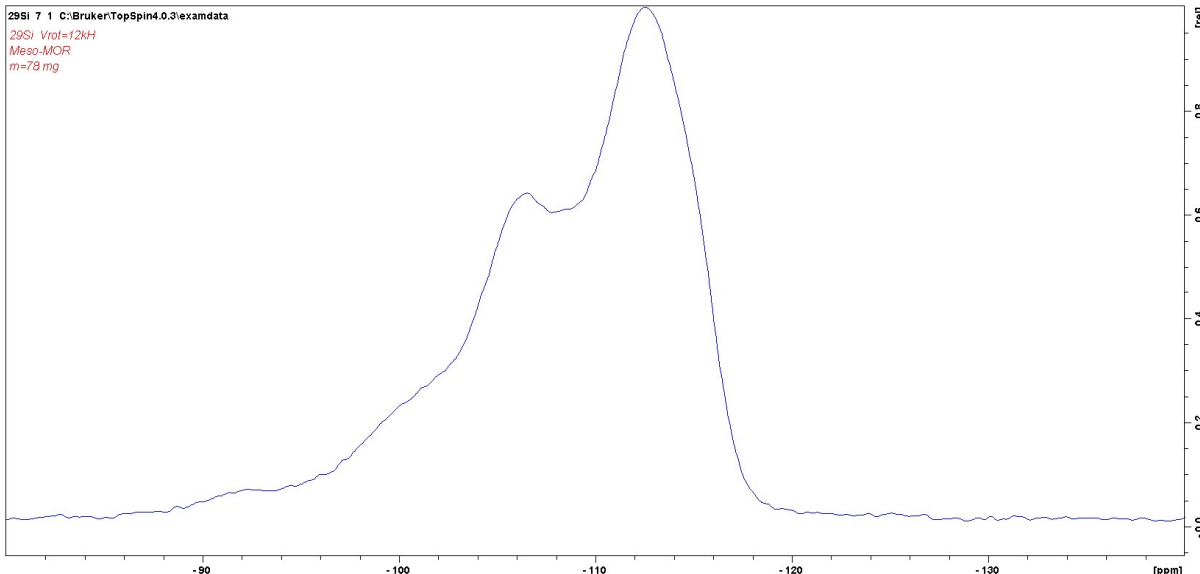


246

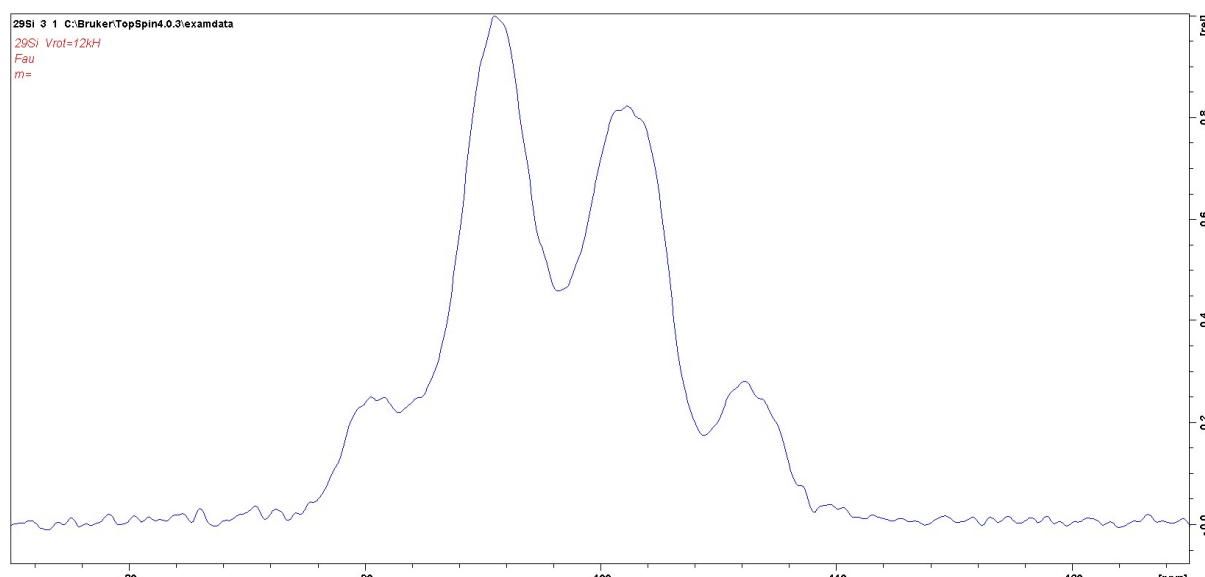
247 **FigureS18e.** <sup>27</sup>Al-NMR spectrum of Na-form of FAU-Z.

248





**FigureS19c.**  $^{29}\text{Si}$ -NMR spectrum of MOR-10.



**FigureS19d.**  $^{29}\text{Si}$ -NMR spectrum of Na-form of FAU-Z.

264 **FTIR spectra of activated zeolites before and after Py adsorption. All spectra were collected**  
265 **at 200°C.**

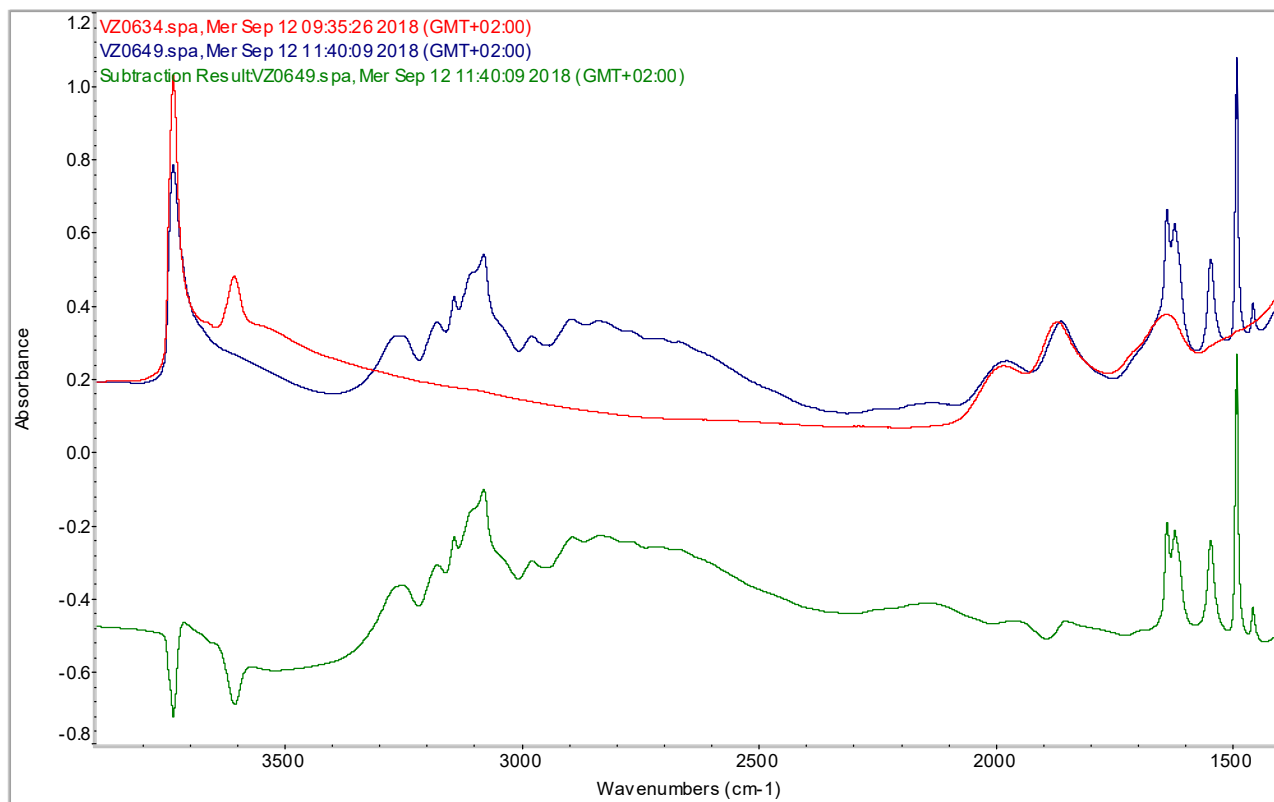


**Figure S20a.** FTIR spectra of BEA-19 **before** and after Py **adsorption**, and the **difference** spectrum.

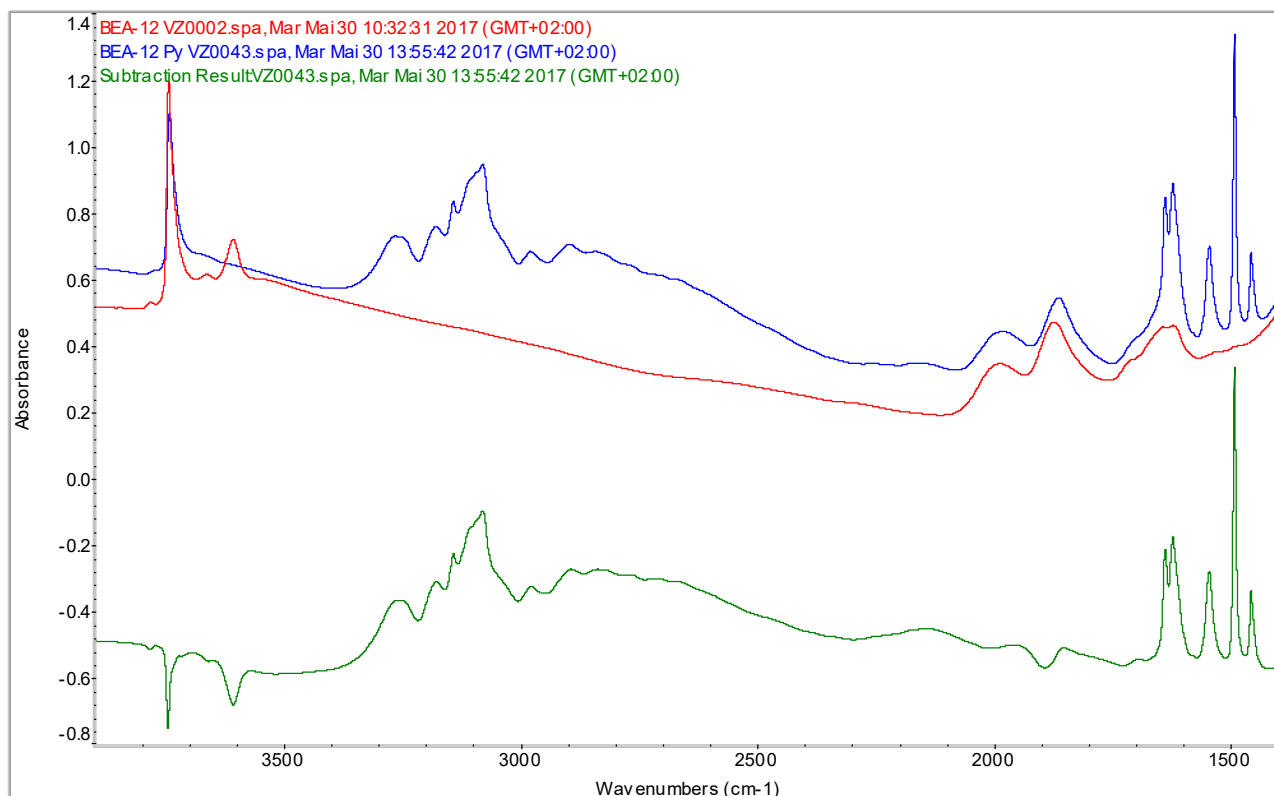


**Figure S20b.** FTIR spectra of BEA-12 **before** and after Py **adsorption**, and the **difference** spectrum.

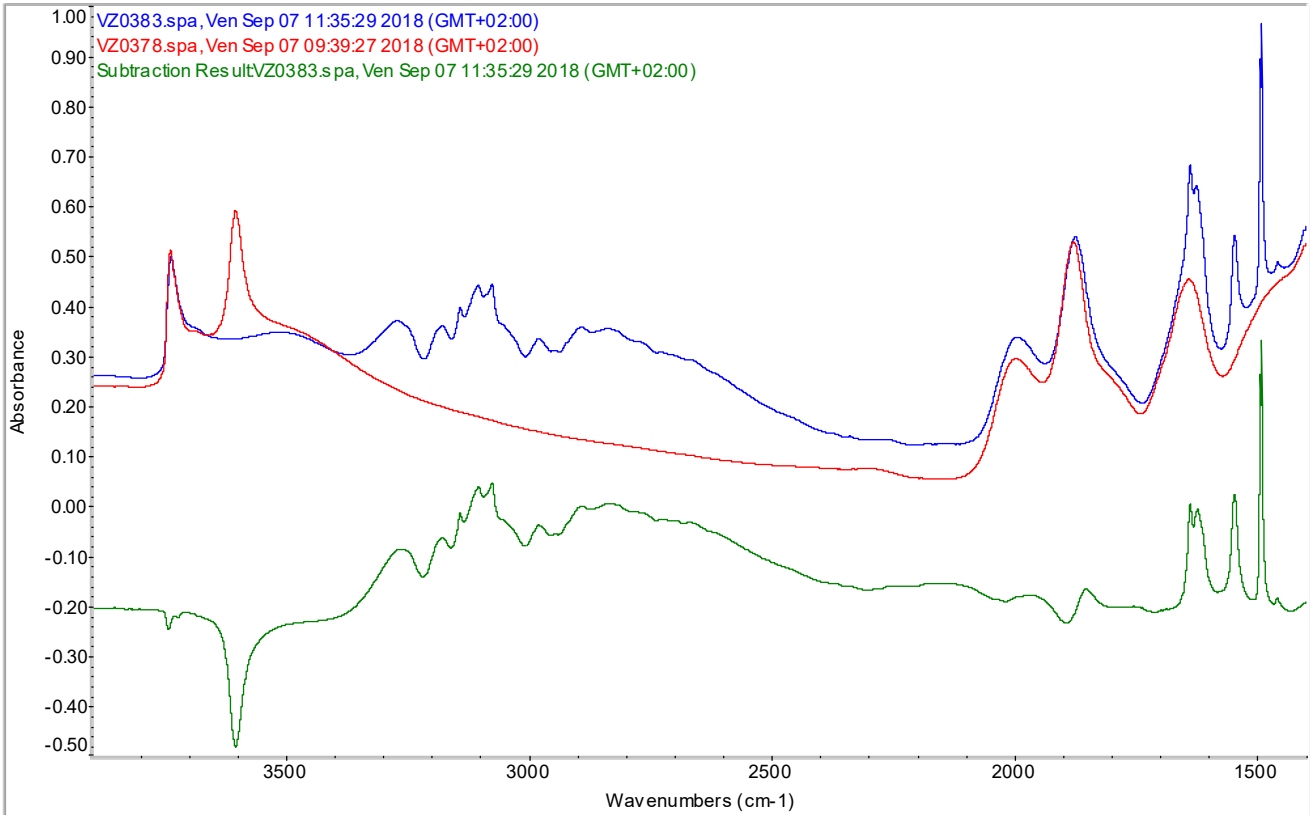


**Figure S20c.** FTIR spectra of ZSM-5-40 **before** and after Py adsorption, and the **difference** spectrum.

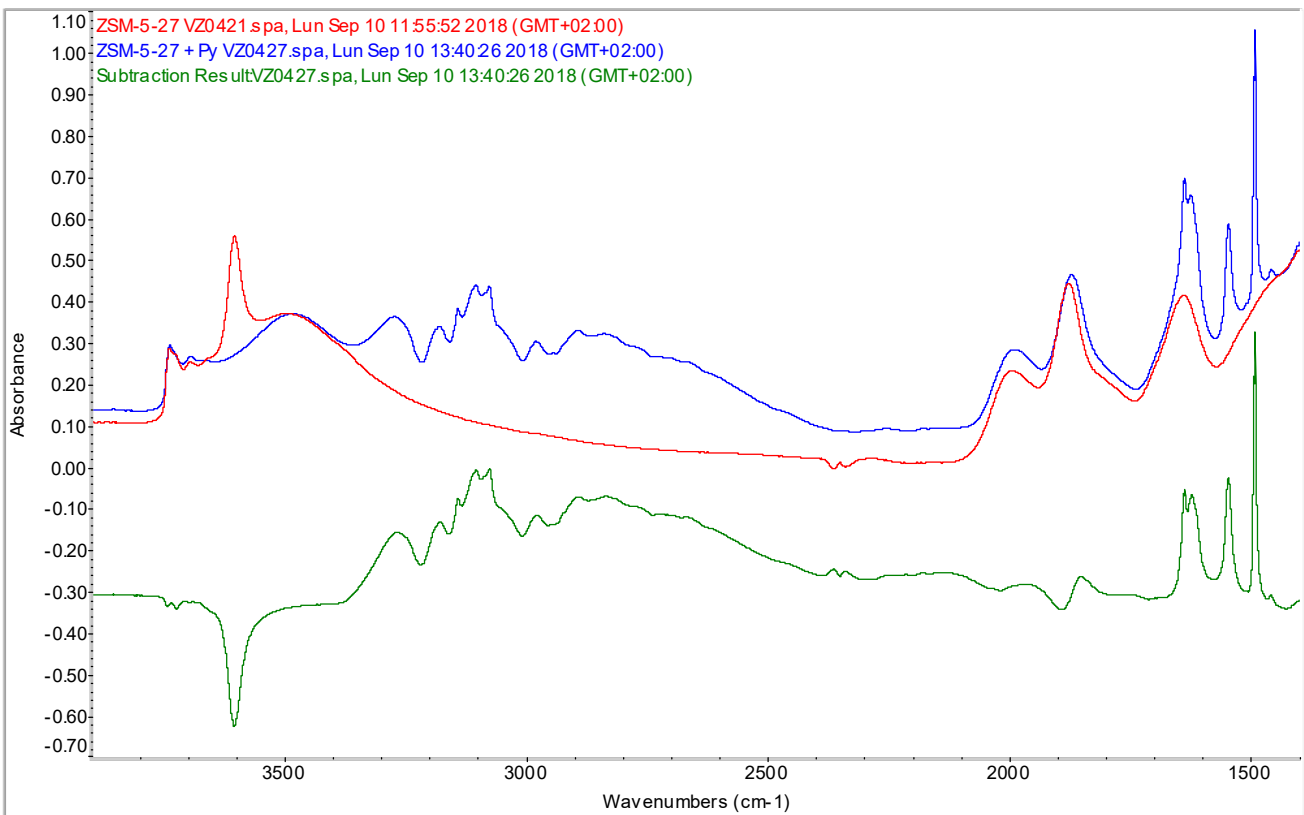


**Figure S20d.** FTIR spectra of ZSM-5-27 **before** and after Py adsorption, and the **difference** spectrum.

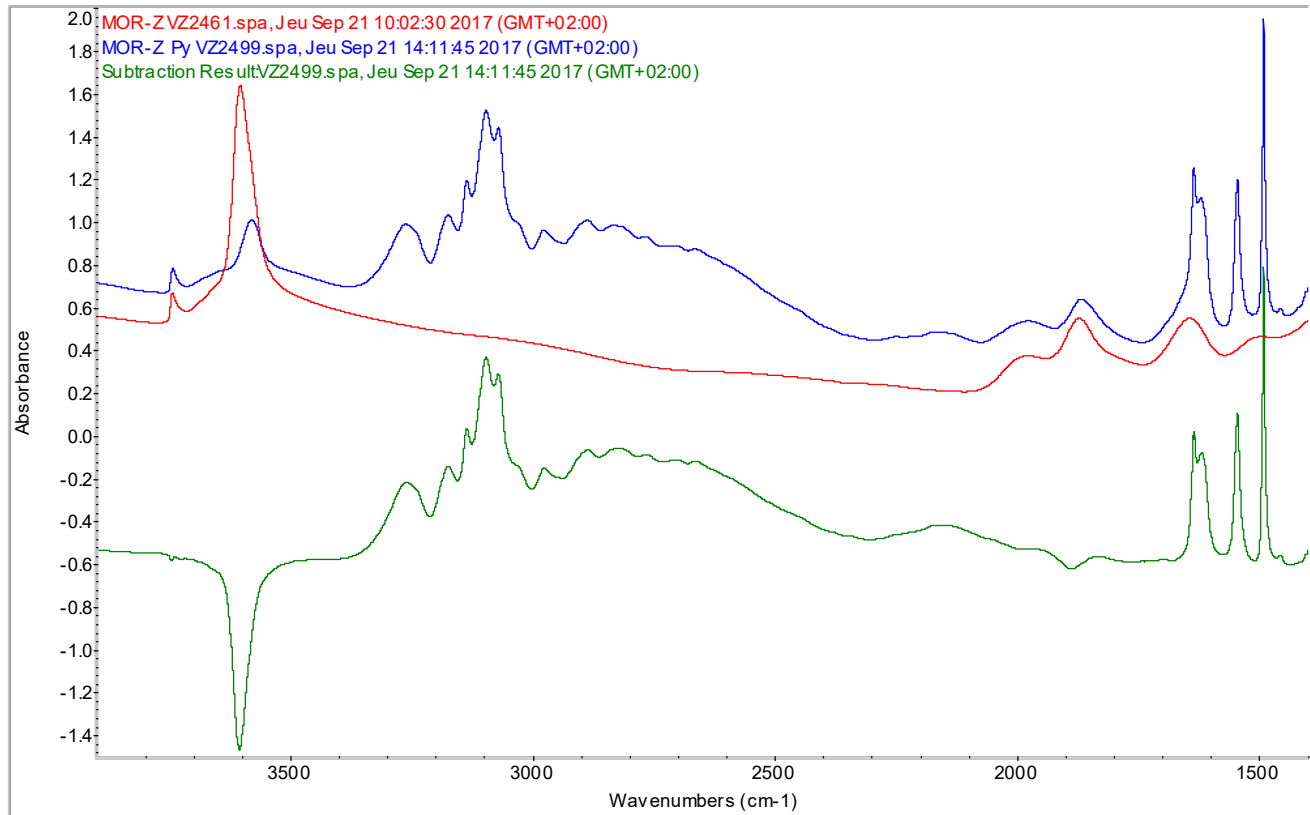


**Figure S20e.** FTIR spectra of MOR-10 **before** and after Py **adsorption**, and the **difference** spectrum.

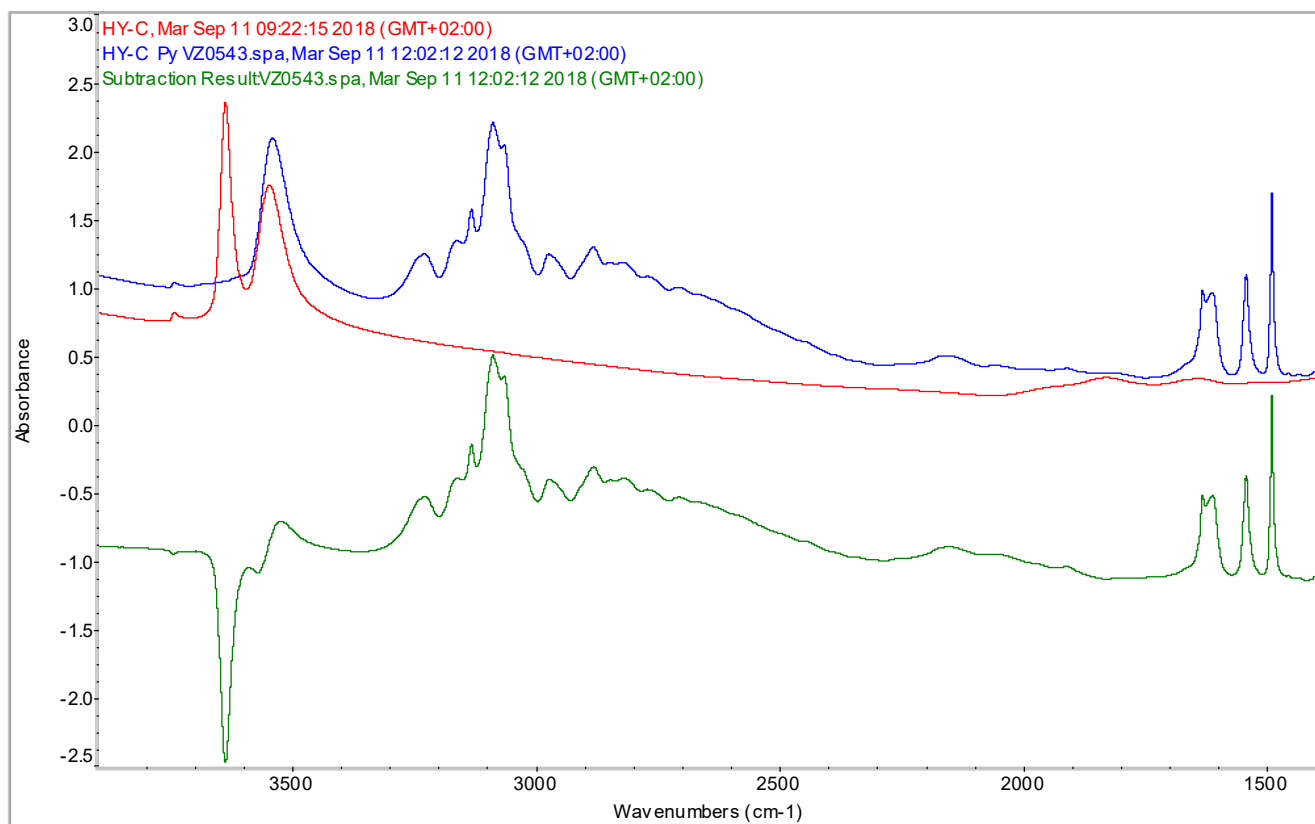


**Figure S20f.** FTIR spectra of FAU-C **before** and after Py **adsorption**, and the **difference** spectrum.

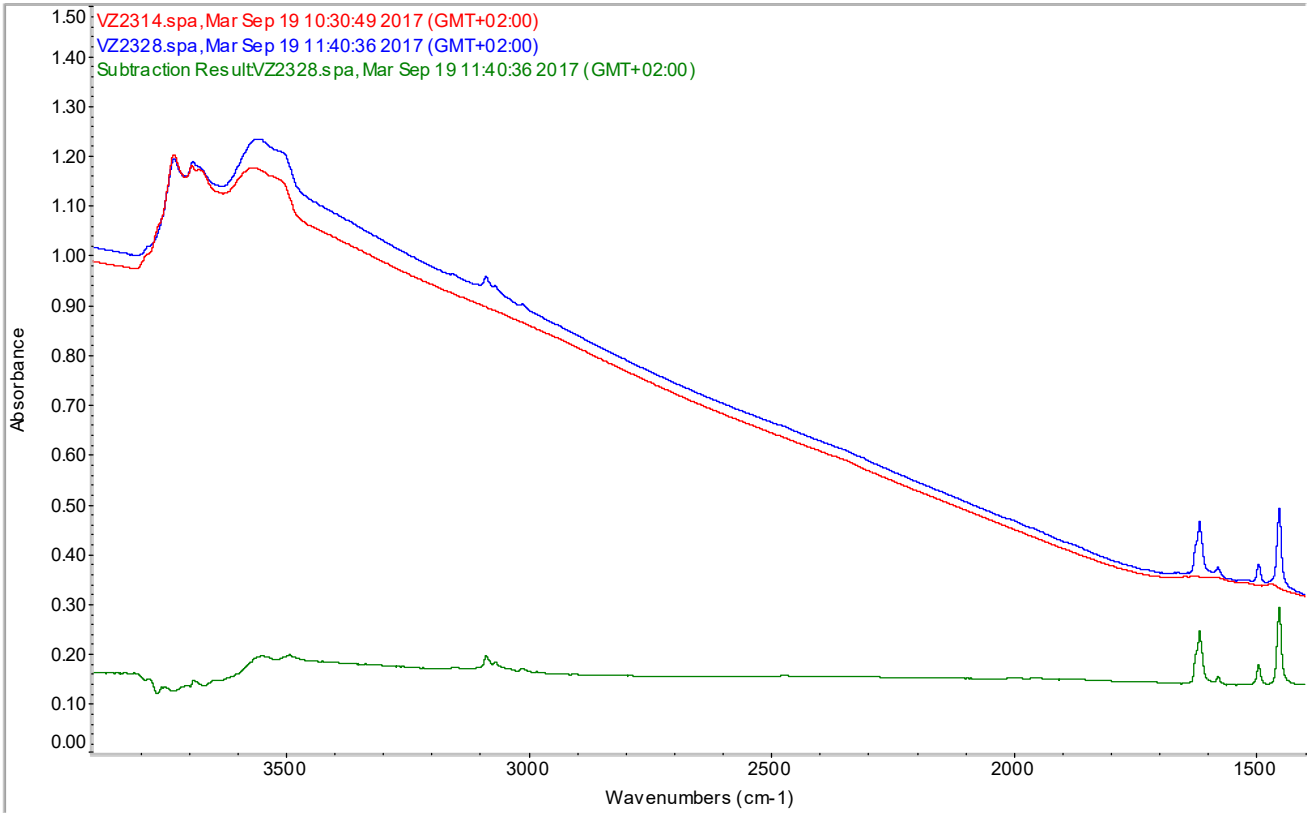


**Figure S20g.** FTIR spectra of  $\gamma$ -Al<sub>2</sub>O<sub>3</sub> **before** and after Py **adsorption**, and the **difference** spectrum.

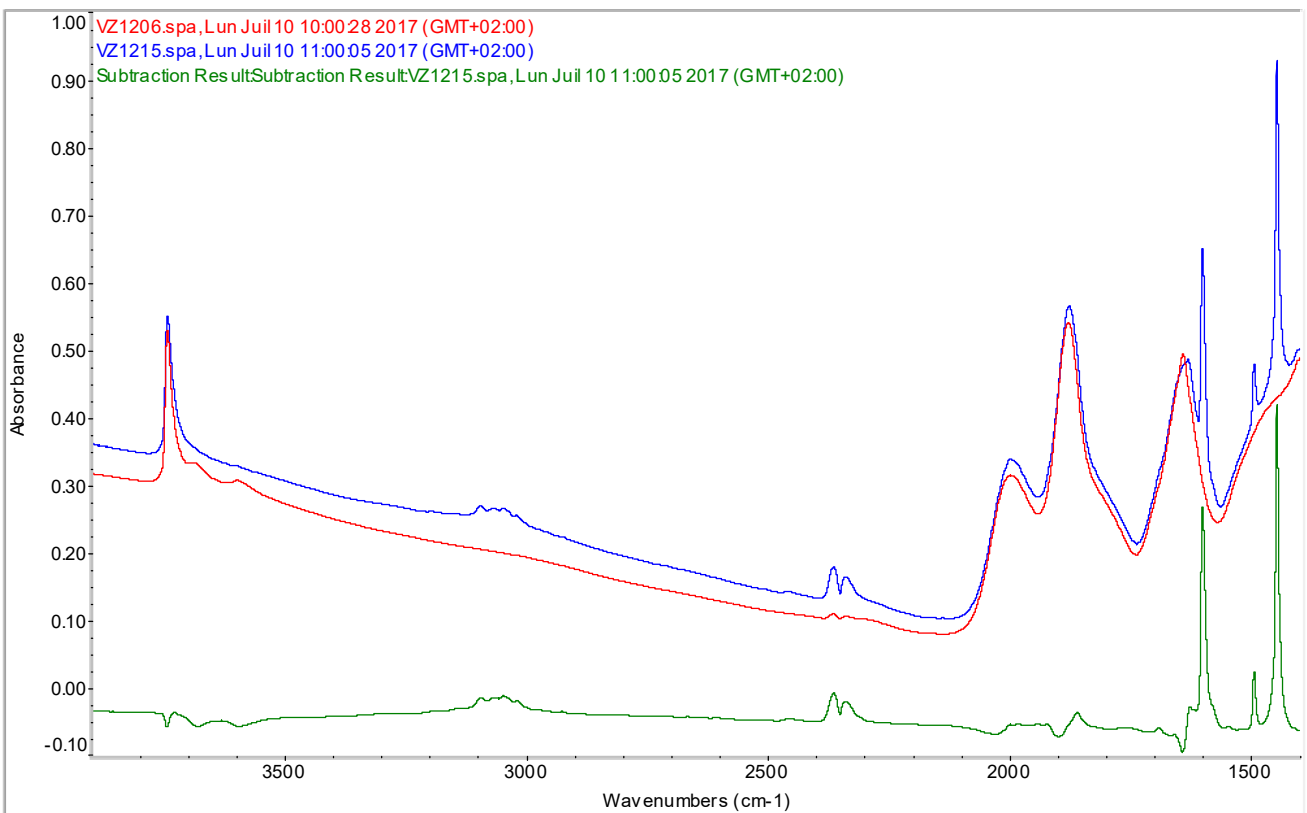


**Figure S20h.** FTIR spectra of NaZSM-5 **before** and after Py **adsorption**, and the **difference** spectrum.